Multiple phase rifting and subsequent inversion in the West Netherlands Basin: implications for geothermal reservoir characterization

Annelotte Weert[1], Kei Ogata[1], Francesco Vinci[2], Coen Leo[3], Giovanni Bertotti[4], Jerome Amory[2], Stefano Tavani[1,5]

[1]Department of Earth, Environmental and Resource Sciences (DiSTAR), University of Naples 'Federico II', Naples, 80126, Italy
[2]PanTerra Geoconsultants B.V., Leiderdorp, 2352BZ, The Netherlands
[3]Geoleo B.V. Consultancy, The Hague, 2596PL, The Netherlands
[4]Faculty of Civil Engineering and Geosciences, Technical University of Delft, Delft, 2628CN, The Netherlands
[5]Consiglio Nazionale delle Ricerche, IGAG, Rome, 00185, Italy

Correspondence to: Annelotte Weert (annelotteweert@gmail.com)

Abstract. Aiming to contribute to the energy transition, this study provides an integrated picture of the geothermal system hosted in the West Netherlands Basin and shows how the reconstruction of the basin's geological history can contribute to the correct exploration and exploitation of its geothermal resources. In the West Netherlands Basin, the main geothermal targets are found in the Cretaceous and Jurassic strata that were deposited during the rifting and post-rifting stages and were deformed during the subsequent basin inversion. Despite multiple studies on the tectonic setting, the timing and tectono-stratigraphic architecture of the rift system and its overall control on the development and evolution of geothermal systems are still to be fully deciphered. In this study, a detailed seismo-stratigraphic interpretation of the syn- and post-rift intervals in the West Netherlands Basin will be given within the framework of geothermal exploration. A recently released and reprocessed 3D seismic cube is used, covering a large portion of the onshore section of the basin. We identified two major Jurassic rifting episodes and a Late Cretaceous inversion event. During the Jurassic rifting phases, the compartmentalisation of the basin and the creation of accommodation space led to the deposition of the Late Jurassic Nieuwerkerk Formation, which is the main regional producing geothermal target. Within this formation, we individuate growth synclines located in the central portions of the Jurassic half-grabens as sites that show good potential for geothermal exploration.

1 Introduction

Subsurface fluid flow systems hosted in rift basins form part of the resources that are indispensable in the global challenge to cut greenhouse gas emissions and cover current and future needs with sustainable energy sources. Basins' bounding faults and the laterally and vertically varying petrological characteristics of their infill, control the distribution, abundance and recoverability of these resources (Gawthorpe and Leeder, 2000). This includes the heat flow needed for high (T > 150°C) to low (T < 90°C) enthalpy geothermal systems (Carapezza et al., 2022). As a frontrunner in Europe, the Netherlands recognizes

the contribution of geothermal energy to be crucial for a successful energy transition (e.g. Kramers et al., 2012; Willems and Nick, 2019; Mijnlieff, 2020).

The West Netherlands Basin (WNB) (Fig. 1) is a former prosperous hydrocarbon province where the interest changed to geothermal energy in the past decade. Having an energy-demanding greenhouse horticulture, a dense population, which includes the cities of Rotterdam and The Hague, and an average geothermal gradient of 31°C km^{-1} (Bonté et al., 2012), the WNB is considered as one of the best case studies for low-enthalpy geothermal exploration (Kramers et al., 2012; Crooijmans et al., 2016; Willems et al., 2017c; Willems, 2017; Vondrak et al., 2018; Willems and Nick, 2019; Willems et al., 2020; Boersma et al., 2021). A typical geothermal project in the Netherlands comprises a low-enthalpy geothermal system for direct heat that contains two or more wells; hot water is produced by production wells and re-injected by injection wells after the heat has been extracted (Limberger et al., 2018). In the WNB, only open loop geothermal systems (i.e. a geothermal doublet that uses the aquifer as heat exchanger) reaching production temperatures ranging from 70°C to 90°C are used (Willems et al., 2017b). For hydrocarbon exploitation in the WNB, an extensive data collection was gathered (e.g. seismic and well data), which is publicly available at https://www.nlog.nl/datacenter/ (e.g. Duin et al., 2006; Kombrink et al., 2012). Up to 2023, 14 geothermal projects were realised in the area (Geothermie Nederland, 2023), targeting aquifers hosted by the post-rift Cretaceous Rijnland Group (two projects), the syn-rift Jurassic Nieuwerkerk Formation (ten projects), and the pre-rift Triassic Buntsandstein (two projects). Financial budgets for geothermal projects are much tighter than for traditional hydrocarbon exploration, making the successful delivery of every well essential to ensure the economic profitability of the geothermal projects. Understanding how the tectonic evolution of a rift basin influences the key parameters used for planning geothermal wells is therefore critical. Such parameters include aquifer thickness and heterogeneity (e.g. Poulsen et al., 2015). A thicker and more homogeneous reservoir allows for better fluid flow, a higher heat extraction and an increased heat recovery (Crooijmans et al., 2016; Willems et al., 2017b), therefore making a geothermal system more profitable. As noted by Willems et al. (2020), current geothermal projects in the WNB demonstrate that the aquifer geology is still not fully understood. Increased knowledge on the regional architecture of the sedimentary formations hosting aquifers, the subsurface geology, and the aquifer properties, would help to de-risk the geothermal well planning in the area (Willems et al., 2020).

Presently, the main target for geothermal exploration in the WNB is the Jurassic Nieuwerkerk Formation (Willems et al., 2017c; Vondrak et al., 2018). This formation was interpreted as deposited in a fluvial-deltaic environment during the main rifting phase that shaped the basin, resulting in sharp lateral thickness and facies variations (van Wijhe, 1987; den Hartog Jager, 1996; Willems et al., 2020). Subsequent basin inversion, which started during the Late Cretaceous, caused uplift and deformation of the Nieuwerkerk Formation (e.g. van Wijhe, 1987; van Balen et al., 2000; de Jager, 2003; Deckers and van der Voet, 2018). This tectonic history makes the reconstruction of the Jurassic tectono-sedimentary sequence, and therefore the thickness of its reservoir rocks more complex.

The quality of the recently reprocessed and released L3NAM2012AR 3D depth migrated seismic cube allows for a detailed reconstruction of the main tectonic structures. In contrast to previous studies that mainly focussed on the NW-part of the onshore WNB (e.g. DeVault and Jeremiah, 2002; Willems et al., 2017c; Vondrak et al., 2018), now the SE-part of the onshore
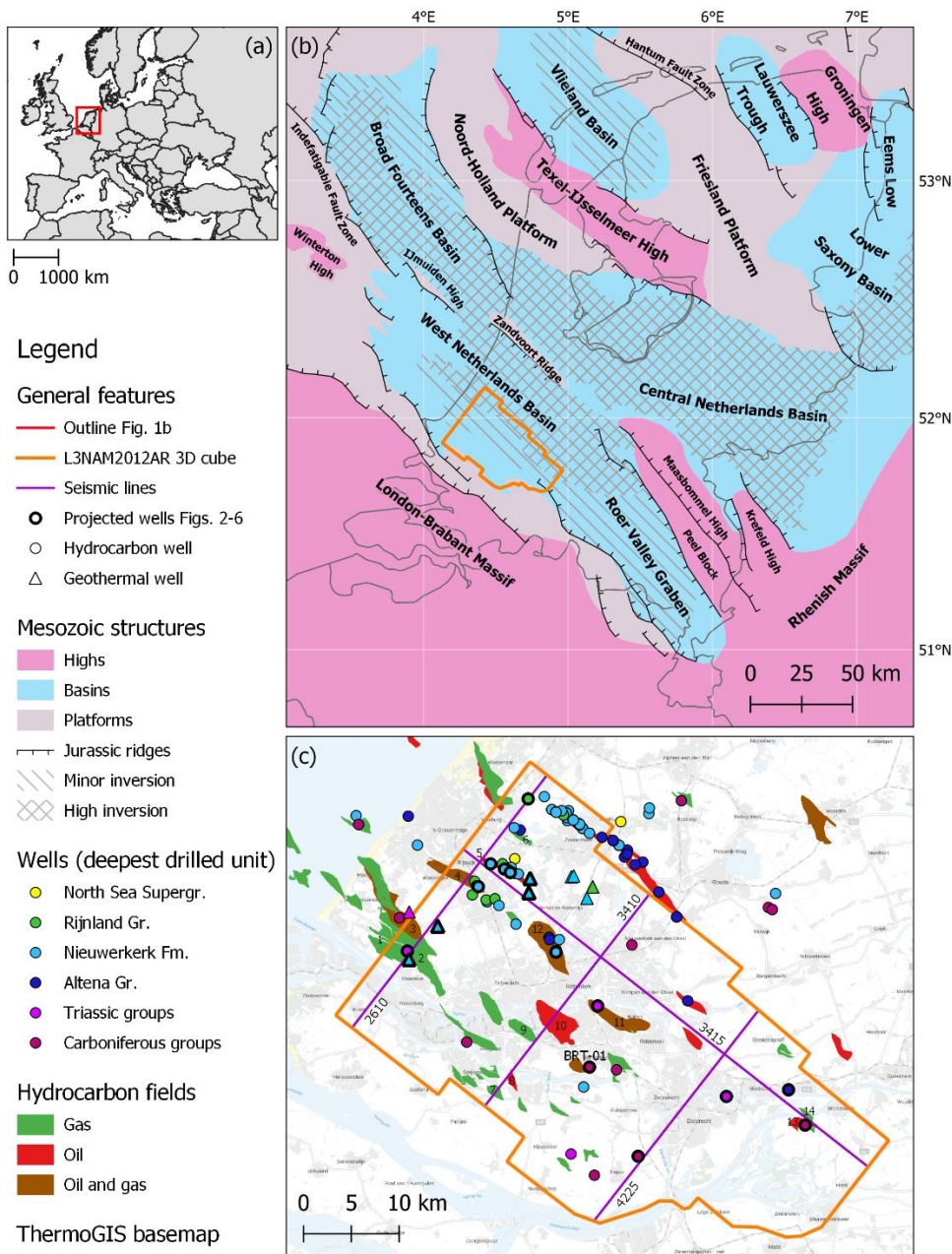
Figure 1: (a) Location of Figure 1b on the European continent. (b) Map of the Netherlands, showing the main structural elements during Jurassic times with the areas affected by the subsequent Late Cretaceous and Cenozoic inversion marked. The 3D seismic cube is displayed in orange. This map was produced by combining the maps from Wong et al. (2007) & Kombrink et al. (2011). (c) Map of the study area, highlighted in orange, showing all used wells with their colours delineating the deepest encountered formation, and the seismic cross sections presented in figures 3 to 6, delineated in purple. Wells presented in figures 2 to 6 are marked by a thicker margin and the hydrocarbon fields mentioned in the Results section of this study are numbered; (1): the Maasdijk field; (2): the Gaag field; (3): the De Lier field; (4): the Rijswijk field; (5): the Pijnacker field; (6): the Leidschendam field; (7): the Hekelingen field; (8): the Oud-Beijerland Noord field; (9): the Pernis field; (10): the Rotterdam field; (11): the IJsselmonde field; (12): the Berkel field; (13): the Werkendam field; and (14): the Werkendam-Diep field.

WNB could be integrated into the study area as well. We use the L3NAM2012AR 3D seismic cube to provide a detailed interpretation of the subsurface geology, improving the knowledge of the structural regional aquifer architecture, with a focus on the Nieuwerkerk Formation.

80
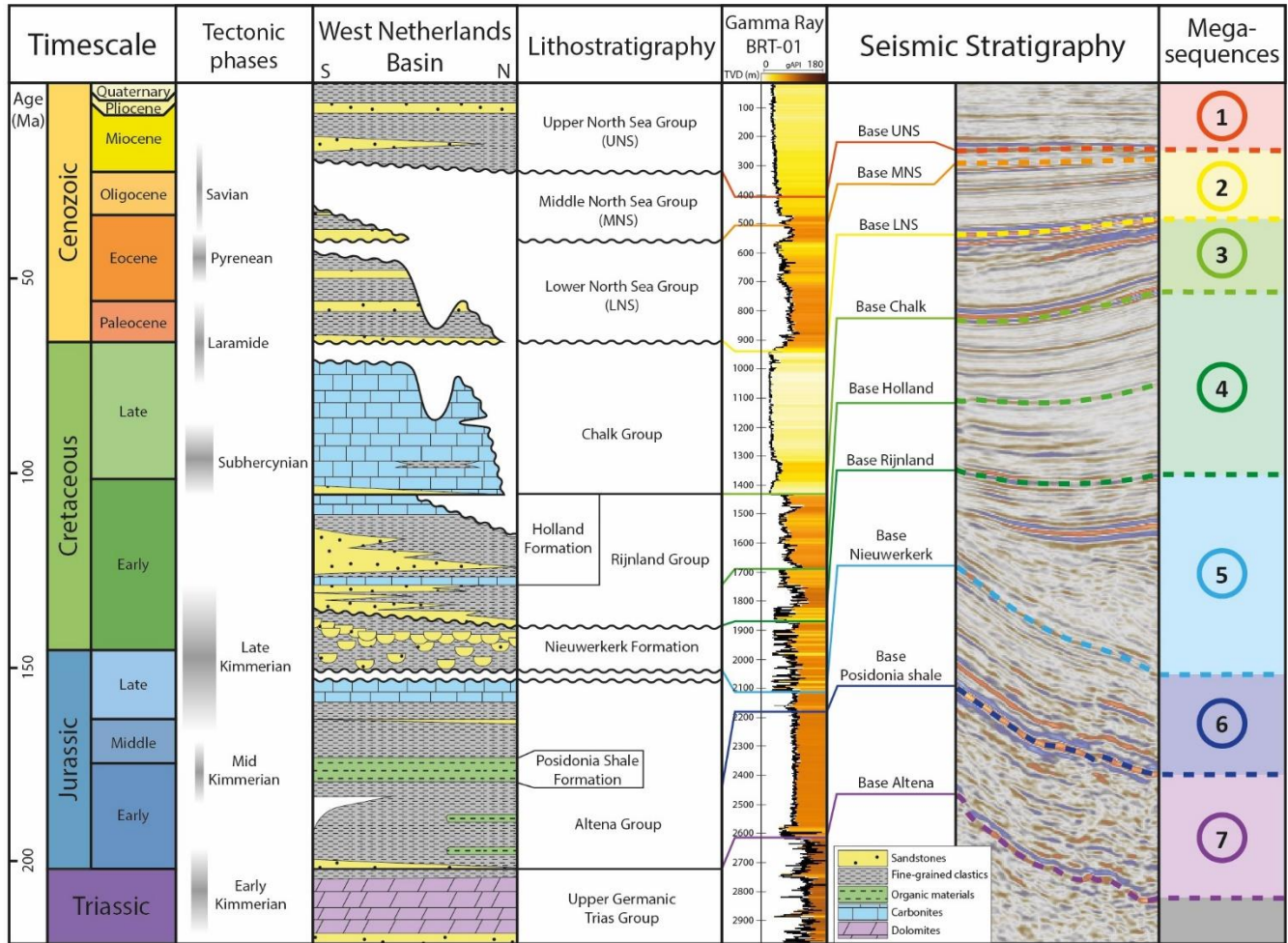
Figure 2: Lithostratigraphic chart, showing the timing of tectonic events, the simplified stratigraphy of the studied section of the West Netherlands Basin, the interpret horizons and their age, the gamma ray log for well BRT-01 that encountered the complete lithostratigraphy, and the typical seismic stratigraphy for the study area. Stratigraphic column adapted from van Adrichem Boogaert & Kouwe (1993) & Jeremiah et al. (2010) and the timing of tectonic events adjusted from Wong et al. (2007) with the results from this study.

85

 2 Geological framework

The West Netherlands Basin (WNB) is a NW-SE elongated basin in the western sector of the onshore Netherlands (Fig. 1). The WNB developed above a former Paleozoic basin, forming part of the Southern Permian Basin, and partly retraces its structural trend (e.g. Ziegler, 1992; van Balen et al., 2000; Michon et al., 2003; Worum et al., 2005). Break-up of Pangea marked the onset of E-W oriented extension in NW Europe at the beginning of the Mesozoic (e.g. Ziegler, 1992). Regionally,

95 the Triassic is characterised by uplift due to the Early Triassic Hardegsen tectonic phase (Geluk et al., 1996) and the Late Triassic Early Kimmerian tectonic phase (Geluk and Röhling, 1997). An Early Jurassic faulting phase is recognized in the area, causing differential subsidence in the basin's various subdomains (van Balen et al., 2000), followed by Middle Jurassic uplift, referred to as the Mid Kimmerian tectonic phase (Herngreen et al., 2003).

Despite the tectonic phases mentioned above, Late Permian to Middle Jurassic times are generally considered to be part of the

100 pre-rift stage within the WNB (e.g. den Hartog Jager, 1996; Racero-Baena and Drake, 1996; van Balen et al., 2000; Vondrak et al., 2018; Willems et al., 2020). The WNB, characterised by horst and graben structures, formed from the Late Jurassic (Kimmeridgian) to Late Cretaceous (Barremian) syn-rift phase (van Wijhe, 1987; den Hartog Jager, 1996; de Jager, 1996; Racero-Baena and Drake, 1996; Vondrak et al., 2018). In particular, the WNB developed during several short discrete pulses, the main one, known as the Late Kimmerian tectonic phase, occurred during the Late Jurassic (van Wijhe, 1987; de Jager,

105 1996; Racero-Baena and Drake, 1996; van Balen et al., 2000). Rifting produced a main NW-SE oriented fault trend and caused the fragmentation of the WNB in several sub-basins, resulting in large thickness variations within the Late Jurassic basin infill. After the end of the rifting phases by the Albian, the WNB underwent post-rift subsidence (van Wijhe, 1987), until basin inversion occurred from the Late Cretaceous to the Miocene (e.g. Ziegler, 1992; de Jager, 2003; Worum and Michon, 2005; Deckers and van der Voet, 2018; Kley, 2018).

110 The Late Permian to Cenozoic sedimentary succession of the WNB, described in detail by van Adrichem Boogaert and Kouwe (1993) and TNO-GDN (2023), starts with the Late Permian Zechstein Group. The very few deep wells that drilled into the Zechstein Group encountered carbonates and shales, but no evaporites. This group is overlain by the Triassic clastic Under-Germanian Group, which includes the Volpriehausen, Detfurth and Hardegsen formations. On top, the Middle to Late Triassic Upper-Germanian Group is made of mixed carbonates and (silici)clastics. Our seismic interpretation focused on the overlying

115 Early to Middle Jurassic Altena Group (Fig. 2), which is primarily composed of shallow-marine clays, but also carbonates and sandstones. The Altena Group includes the Posidonia Shale Formation, which forms a key seismic reflector (Fig. 2). In the study area, the overlying Late Jurassic-Early Cretaceous Schieland Group includes only the Nieuwerkerk Formation, which is one of the main targets for geothermal exploration in the WNB (see above). It is characterised by lateral thickness variations associated with extensional faulting, and includes sandstones and shales that are both vertically stacked and laterally

120 interfingered. The overlying Cretaceous Rijnland Group includes the Vlieland Subgroup and Holland Formation. The clastics of the Vlieland Subgroup were deposited in a transgressional setting that turned into a shallow to deep marine environment in which the carbonate and siliciclastic sediments of the Holland Formation were deposited. The Late Cretaceous carbonates of

the Chalk Group were deposited in a shallow marine environment during the main inversion phase. The Cenozoic succession is known as the North Sea Supergroup, composed of the clastics of the Lower, Middle and Upper North Sea Groups (e.g., van Adrichem Boogaert and Kouwe, 1993; Duin et al., 2006).

125

3 Data and methods

This study uses the L3NAM2012AR 3D seismic depth cube and well data (Fig. 1c), which is publicly available and can be downloaded from https://www.nlog.nl/datacenter/. Additional technical details, including the reprocessing report and the acquisition, processing and interpretation work that was done before the reprocessing, can be found on the same website, using

130   the provided steps described in the Supplementary Materials. The seismic coverage has a surface area of roughly 1200 km^2, with 2678 diplines (2500-5178) and 1714 strikelines (2273-3987), penetrating to a depth of 6 km. The 3D cube was depth reprocessed and converted by Shell in 2011, using 59 wells for the depth conversion. We will use the depth converted version of this seismic cube, as the velocity cube was not publicly available (on the first of September 2023). Additional wells are available, from which we have used a total of 94 inside and 31 close to the study area, with a maximum depth of 4 km, and

135   the deepest drilled formation being the Carboniferous Limburg Group (Fig. 1c). Specifically, for those wells, the gamma ray logs in combination with the available formation tops made it possible to tie the wells to the seismic data (Fig. 2). This allowed the calibration of the age of the main seismic horizons and sequences. Yet, some of the used wells dated back to the start of hydrocarbon exploration in the basin during the 1950's. With the lithostratigraphic nomenclature changing over time, not all available formation tops are matching. This includes formation and group boundaries that are not used anymore. Therefore,

140   unmatching well tops were neglected.

We performed the seismic analysis and interpretation using Petrel 2020.3 software, following the well-established workflow for interpretation of seismic datasets in extensional settings (e.g. O'Sullivan et al., 2022). We interpreted the main faults and defined the seismic stratigraphy by integrating the well data in order to date the main seismic units (megasequences in this work), unconformities, and brightly marked reflective horizons. In detail, nine horizons were interpreted for the whole 3D

145   cube (Fig. 2). Such a 3D interpretation has allowed us to define the main megasequences of the basin and produce thickness maps of the pre-, syn-, and post-rift deposits, shedding light on the tectono-sedimentary evolution of the sub-basins.

The nine horizons were selected either for their easily recognizable seismic facies or for their structural appearance (e.g. unconformities). To date the interpreted seismic horizons, we relied on seismic to well ties to calibrate the seismic horizons with the well tops provided by TNO on nlog.nl. In particular, the bases of the Cenozoic Upper, Middle and Lower North Sea

150   Groups form angular unconformities, all easily recognized by their bright troughs that match the provided well tops very well (e.g. Figs. 2 and 5). The clastic package of this Supergroup is defined by sub-horizontal, parallel reflectors. The base of the upper Cretaceous Chalk Group is represented by a bright peak that is easy to track, lying mainly conformable over the underlying strata, with some local unconformable contacts (e.g. Fig. 5). The Chalk Group comprises sub-horizontal reflectors in its upper part, showing some local folds in its central and lower parts that are separated from the overlying reflectors by a

155 local unconformity. The base of the lower Cretaceous Holland Formation, part of the Rijnland Group, is defined by a trough that conformable overlies the Vlieland Subgroup. The base of the Rijnland Group is defined by a minor peak that is not easy to track. We used the well tops to interpret this horizon inside the sub-basins. The marine infill of the Rijnland Group includes parallel reflectors, affected by faults and folds (e.g. Fig. 4). Overall, the reflectors of the Holland Formation show a higher amplitude than the underlying unit of the Rijnland Group (e.g. Fig. 3). The base of the upper Jurassic Nieuwerkerk Formation

160 is defined by a bright trough which is easy to track along the sub-basins using the provided well tops. Overall, the Nieuwerkerk Formation lies conformably upon the underlying Altena Group, yet some unconformable contacts are present (e.g. Fig. 4). The package shows a range of seismic facies; going from bright parallel to chaotic reflectors. The bases of the Posidonia Shale Formation and the Altena Group are easy recognizable as bright troughs. The Altena Group, which includes the Posidonia Shale Formation, comprises bright and dull parallel reflectors, with some chaotic reflectors locally, all affected by faults and

165 folds (e.g. Fig. 5).

For each horizon, a grid of 25 diplines x 25 strikelines was made using a guided approach (guided autotracking + seeded 3D tools of Petrel). A continuous checking of the geological consistency of the interpretation was carried out during the interpretation, by considering the seismic facies of the mapped horizons and the occurrence of regional unconformities, as illustrated in Figure 2. The Results section describes three diplines and one strikeline that cover the study area and are

170 considered representative for all structures found in the 3D seismic cube (Figs. 3-6). All four seismic sections were flattened for the base of the Rijnland Group. Despite all the limitations and biases of the flattening procedure, the flattened sections provide insights in the thickness variations of the Rijnland Group and underlying Nieuwerkerk Formation. Also, we build thickness maps for megasequences 2 to 7 respectively (Fig. 2); the Middle and Lower North Sea Groups combined (Fig. 7b), the Chalk Group (Fig. 7c), the Rijnland Group (Fig. 7d), the Nieuwerkerk Formation (Fig. 7e), the upper half of the Altena

175 Group (up to the base of the Posidonia Shale Formation, Fig. 7f) and the lower half of the Altena Group (Fig. 7g). The thickness map for each unit was produced in Petrel by computing the difference in elevation between the bounding horizons. Although such a difference is not the actual thickness, given the horizons are characterised by a very gentle dip (mostly less than 5°), it represents a reliable proxy. Exceptions are those areas of steeply dipping layers associated with tight folds. Also, the difference in elevation returns artefacts across faults, in which the top and bottom horizons are located in the hanging wall and footwall,

180 respectively. Those two exceptions are recognisable in maps as narrow ribbons of anomalous thickness values, mostly overlapping the major faults. A depth map was produced for the Upper North Sea Group (Fig. 7a), corresponding to the uppermost megasequence 1 (Fig. 2).
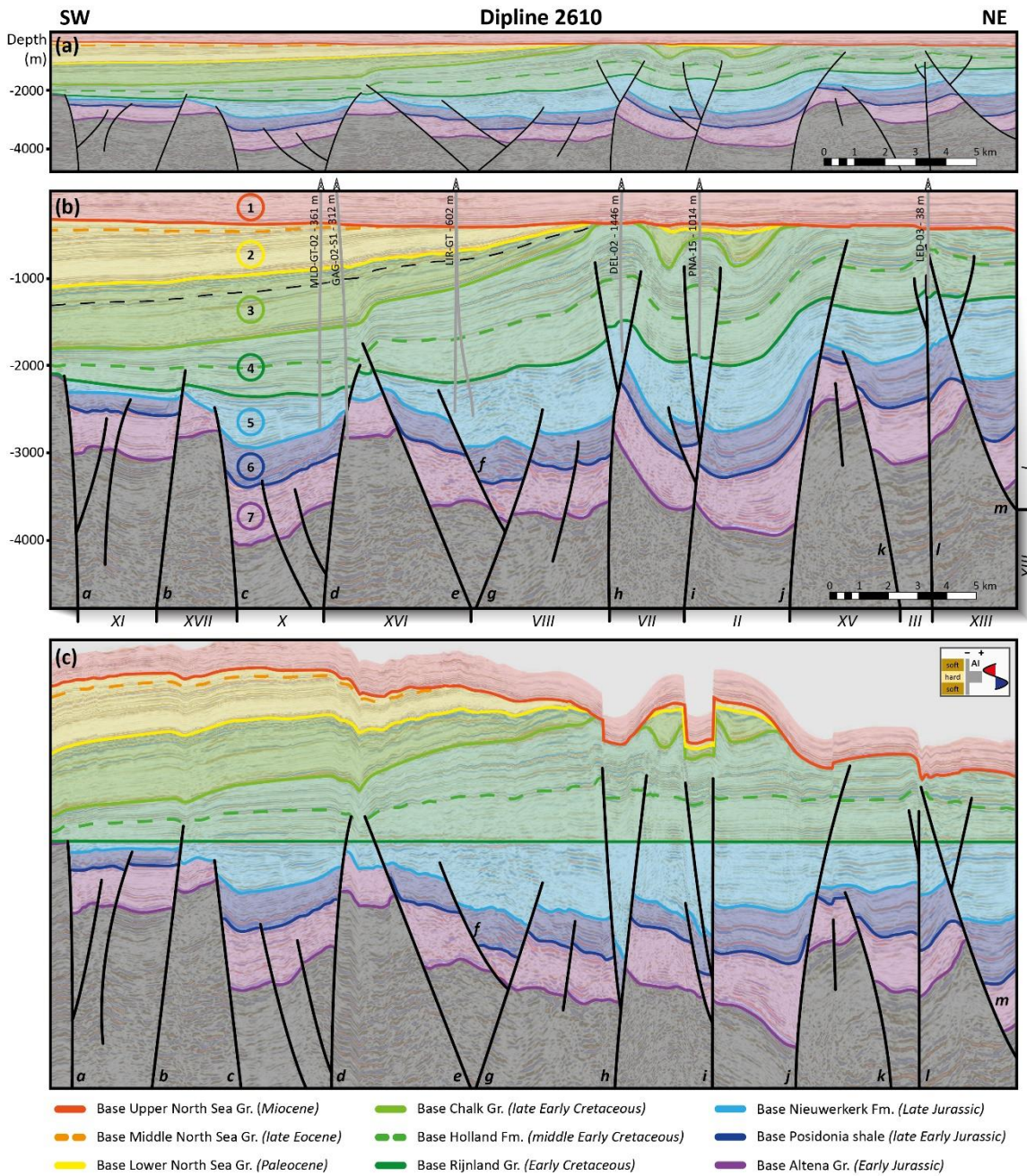
Figure 3: Dipline 2610 displayed with three different scales; (a): 1:1 scale, displayed with the interpreted horizons, megasequences and faults; (b): 1:3 scale, displayed with the interpreted horizons, megasequences and faults, together with projected wells and their distance to the seismic line, and the unconformity within megasequence 3 (marked by the black dotted line). Below the section, the sub-basins and highs are numbered as in Figure 7 ((XI): Voorne Graben, (XVII): Hoek van Holland High, (X): Maasland Graben, (XVI): De Lier High, (VIII): Westland Graben, (VII): Rijswijk Graben, (II): Voorburg Graben, (XV): Zoetermeer High, (III): Zoetermeer Graben, (XIII): Moerkapelle High, (I): Waddinxveen Graben); (c): the 1:3 scaled section flattened for the base of the Rijnland Group, displayed with the interpreted horizons, megasequences and faults.

4 Results

4.1 Seismic sections

Here we present three SW-NE sections oriented perpendicular to the main trend of faults affecting the WNB, and one section oriented NW-SE (Fig. 1c). Up to the top of the Triassic, the stratigraphic succession can be divided into seven megasequences,
195   here described from top to bottom. For each section, we present a 1:1 and 1:3 vertically exaggerated interpreted lines, along with a 1:3 vertically exaggerated one, flattened to the base of the Rijnland Group. The non-interpreted sections can be found in the Supplementary Materials.

4.1.1 Dipline 2610

Dipline 2610 (Fig. 3) is located on the NW edge of the study area. The section is crosscutting the Pijnacker (PNA-15) and
200   Rijswijk (DEL-02) abandoned oil fields, and the Maasdijk, the Gaag (GAG-02-S1) and the De Lier (LIR-GT wells) producing gas fields. The Leidschendam (LED-03) abandoned gas field and two producing open loop geothermal energy projects (MLD-GT-02 & LIR-GT wells) are nearby (hydrocarbon fields 1 to 6, Fig. 1c).

Megasequence 1 is positioned between the top of the seismic cross-section and the base of the Upper North Sea Group. The package is characterised by sub-horizontal reflectors and an evident erosional surface at the bottom, forming an angular
205   unconformity and a toplap surface. Megasequence 2 underlies this erosional surface, towards the SW. This megasequence is eroded in the NE part of the section and contains the Middle and Lower North Sea Groups. To the SW, the package is slightly tilted, dipping a few degrees towards the SW. Towards the SW, reflectors of megasequence 2 and 3 are parallel, whereas megasequence 2 eroded the top of megasequence 3 in the Westland Graben (structure VIII, Fig. 3b). This leaves a local angular unconformity between megasequences 2 and 3 (the unconformity is also found in well PNA-15, Fig. 3b). Around well PNA-
210   15, we observe two growth synclines capped by the unconformity that underlies megasequences 1 and 2. Megasequence 3 is composed of the Chalk Group, which thins from 700 to 0 m towards the NE. The upper part of megasequence 3 is locally separated from the central and lower ones by an unconformity (dashed black line, Fig. 3b). The apparent NE-ward thinning of this megasequence resulted from erosion, which is marked by the erosional surface at the base of megasequence 1. The underlying megasequence 4 comprises the Rijnland Group. In contrast with megasequences 2 and 3, this package thins
215   gradually from 1000 to 350 m towards the SW and it is affected by synclines and fault-cored anticlines. Despite some local thickness anomalies (associated with the flattening procedure and the presence of faults) the flattened profile corroborates the regional thinning of megasequence 4 towards the SW, which is not considerably affected by the faults and folds observed in the non-flattened profiles (Fig. 3). It is worth mentioning that observed major faults affect the upper part of megasequence 4 and megasequences 5, 6 and 7, with the youngest three megasequences being un-faulted. Megasequence 5, which corresponds
220   to the Nieuwerkerk Formation, is characterised by abrupt thickness changes (from 100 to 900 m) across the numerous faults affecting the megasequence. Below, megasequence 6, composed of the upper part of the Altena Group, and underlain by the Posidonia Shale Formation, is characterised by parallel reflectors and thickness variations from 700 to 0 m, which relate to

erosion atop structural highs. Finally, megasequence 7, comprising the lower part of the Altena Group, displays both parallel reflectors and a few growth geometries at fault-bounded sub-basins.

225 The seismic line crosses 12 major faults. Some of them display normal offsets, while others show normal offset in the lowermost tracts and reverse displacement in the upper portions, which is a diagnostic feature of fault inversion (Williams, 1989). All major faults affect the megasequences 5 to 7, whereas only those showing evidence of positive inversion propagate into megasequence 4. As previously mentioned, megasequences 1 to 3 are un-faulted. In detail, faults labelled *a* to *d*, define horst and graben/half-graben structures. In the grabens/half-grabens, megasequence 5 shows growth geometries, whereas in

230 the horst, the thickness of megasequences 5 to 7 is strongly reduced from 1400 m in the graben to 550 m on the adjacent horst. None of these faults show remarkable evidence of inversion and the lowermost part of megasequence 4 seals all of them. Faults *e* and *h* bound a pop-up structure resulting from the inversion of these two former normal faults and the uplift of the pre-existing sub-basin depocenter. Faults *f* and *g*, which show no evidence of inversion, were part of the array of extensional faults within this depocenter. In detail, the inversion of the SW boundary fault *e* caused fault-propagation-folding registered by

235 'contractional' growth strata in megasequence 3. Inversion of the NE boundary fault *h* was accompanied by the development of an antithetic fault, forming a second-order pop-up structure that affected megasequence 4. To the NE, the SW-dipping fault *i* is syn-sedimentary with respect to megasequence 5. Its inversion is accompanied by the development (or inversion) of two conjugate NE-dipping faults and resulted into a second-order pop-up structure, which controlled the deposition of megasequence 3. Fault *j* displays evidence of positive inversion and, more importantly, bounds a half-graben (the Voorburg

240 Graben, structure II, Fig. 3b) in which megasequence 7 displays growth-wedge geometries. The NE-dipping fault *k* also bounds the Zoetermeer Graben (structure III, Fig. 3b) in which the thickness of megasequence 5 varies from 400 to 500 m and the thickness of megasequence 7 changes from 500 to 600 m. Accordingly, the fault was active during the deposition of megasequences 5 and 7. It is worth mentioning that it was not reactivated during later inversion. Fault *l* is NE-dipping and was active during deposition of megasequence 5. This is evidenced by the flattened section, showing that megasequence 5 is about

245 100 m thicker on the NE-side of fault *l* (Fig. 3c). Fault *l* shows slight inversion, as suggested by the gentle anticline deforming megasequence 4. Apart from the clear evidence of reverse offset on normal faults, folding of reflectors both in the hanging wall and footwalls of some faults (e.g. in the footwall of fault *l* or in the hanging wall of faults *e* and *k*), reveals a possible buttressing effect (i.e. folding and second order faulting on the hanging wall and footwall without slip reversal along the master fault).

250 **4.1.2 Dipline 3410**

Dipline 3410 (Fig. 4) is located 16 km to the SE of dipline 2610. The section crosses the Rotterdam and Oud-Beijerland Noord producing oil fields and the Pernis and Hekelingen producing gas fields. Close-by are the IJsselmonde (IJS-64-S2) and Berkel (BRK-07) abandoned oil fields (hydrocarbon fields 7 to 12, Fig. 1c).

Megasequence 1 shows sub-horizontal reflectors underlain by a regional erosional surface. In the SW part of the section, the
255 underlying megasequence 2 shows gently tilted to parallel reflectors that are eroded towards the NE. An unconformable contact

separates megasequences 2 and 3, the latter shows a substantial thinning from 700 to 0 m towards the NE. Megasequence 3 forms low-amplitude synclinal and anticlinal structures, which are well defined at its base and are capped by the unconformable overlying megasequence 2. Similarly to the seismic line shown in Figure 3, we observe a gently folded unconformity between the uppermost part and the central and lower parts of megasequence 3 (black dashed line in Fig. 4b). Megasequence 4 shows parallel reflectors thinning from 1000 to 200 m towards the SW (Figs. 4a and c), which are disrupted by faults. In the NE part of the section, the megasequence is partly eroded and directly toplapping onto megasequence 1. Major faults cut megasequence 4 above the base of the Holland Formation, and megasequences 5, 6 and 7, while the youngest three megasequences are un-faulted. Megasequence 5 is affected by faults *d*, *n*, *h*, *o*, *i* and *k*, displaying abrupt thickness changes ranging from 400 to 1300 m. These thickness changes are even more clearly visible on the flattened section. The package shows at least four distinct asymmetric fault-bounded half-grabens. The underlying megasequence 6 is characterised by parallel reflectors and, contrasting with section 2610, megasequence 6 does not show significant thickness changes, having an average thickness of 450 m. The lowermost megasequence 7 displays both parallel layers, slight thickness changes (ranging from 500 to 850 m), and a fault-bounded half-graben in the Zoetermeer Graben (structure III, Fig. 4b).

Seven major faults are recognized in this seismic section, both normal and partially (in the lowermost tracts) inverted faults. The faults cut megasequences 5 to 7, whereas only the faults showing positive inversion cut through megasequence 4. Faults *c*, *d*, *h*, *i* and *k*, recognized in dipline 2610, are also mapped in this section. In detail, faults *c* and *d* bound a structural high (the De Lier High, structure XVI, Fig. 4b), describing small horst and graben structures. Megasequence 5 is absent in this region and the horst and graben, and the bounding faults are sealed by the uppermost part of megasequence 4. Fault *c* and minor related faults show notable evidence of inversion, marked by the antithetic fault connected to fault *c*. However, contrasting with section 2610, where fault *d* does not display evidence of inversion, the inversion of this fault in this section resulted in the development of antithetic fault *n*. Together, the faults formed a set of small pop-up structures, recorded by a fault-propagation fold atop fault *n* in megasequence 4. The SW dipping faults *h* and *i* show a similar geometry, being controlled by the deposition of megasequence 5. Inversion of both faults was accompanied by the development of fault-propagation folds in megasequence 4. Both faults formed second-order pop-up structures in section 2610. Faults *h*, *i* and *o* bound the Rijswijk and Pijnacker grabens (structures VII and IV, Fig. 4b). In these structures, megasequence 5 shows clear growth geometries. Inversion of fault *o* caused the development of an antithetic fault, forming a second-order pop-up structure. The growth geometries in megasequence 3 recorded the development of the fault-propagation folds and the second-order pop-up structure as result of the inversion of faults *d*, *h*, *o* and *i*. Fault *k* bounds the Zoetermeer Graben (structure III, Fig. 4b) in which megasequences 5 shows thickness variations ranging from 600 to 800 m and megasequence 7 displays thickness changes from 800 to 400 m. Like in section 2610, folded reflectors (e.g. in the hanging wall of fault *d* and footwall of fault *i*) suggest a buttressing effect upon inversion.
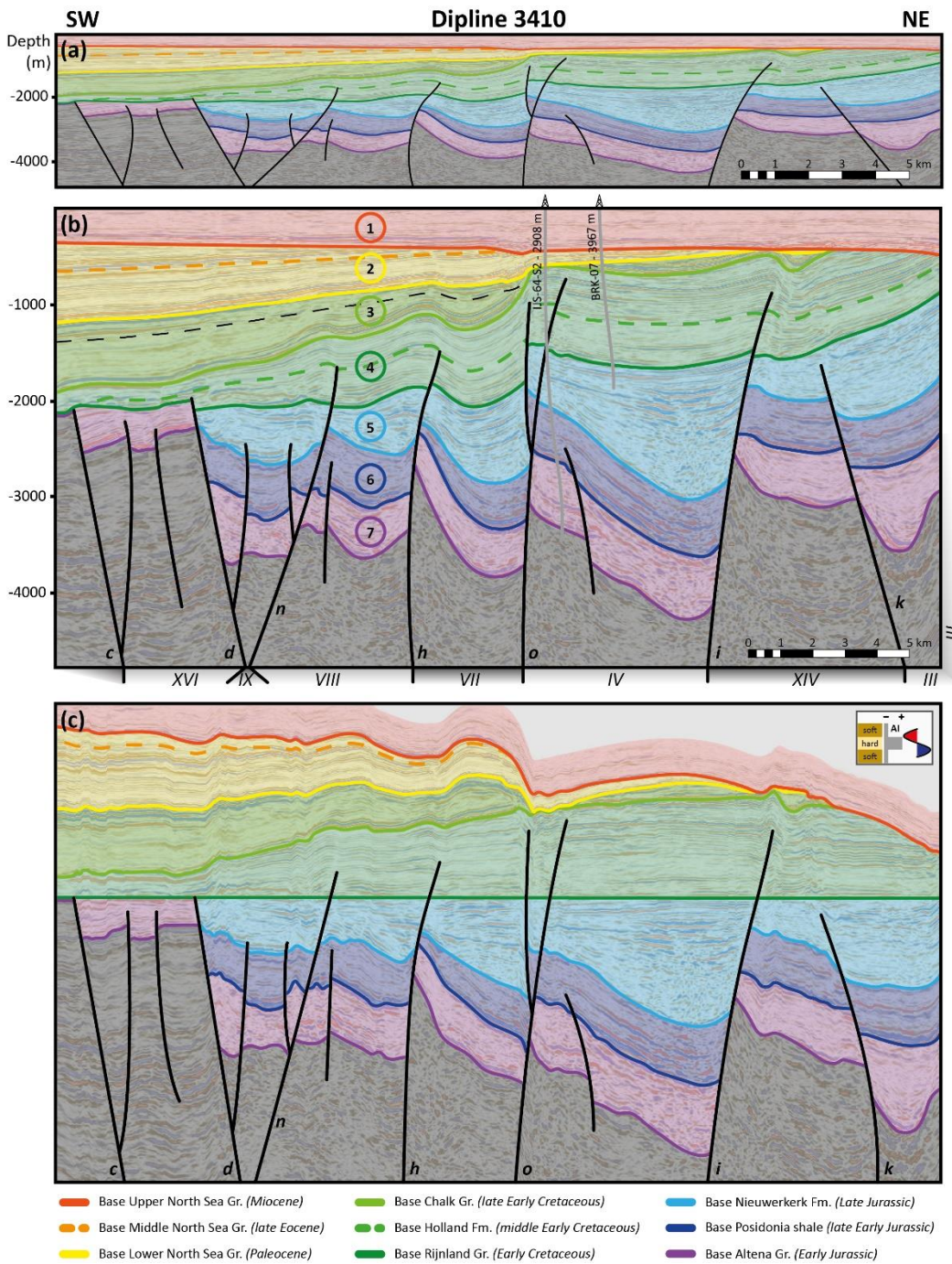
Figure 4: Dipline 3410 displayed with three different scales; (a): 1:1 scale, displayed with the interpreted horizons, megasequences and faults; (b): 1:3 scale, displayed with the interpreted horizons, megasequences and faults, together with projected wells and their distance to the seismic line, and the unconformity within megasequence 3 (marked by the black dotted line). Below the section, the sub-basins and highs are numbered as in Figure 7 ((XVI): De Lier High, (IX): Spijkenisse Graben, (VIII): Westland Graben, (VII): Rijswijk Graben, (IV): Pijnacker Graben, (XIV): Lansingerland High, (III): Zoetermeer Graben); (c): the 1:3 scaled section flattened for the base of the Rijnland Group, displayed with the interpreted horizons, megasequences and faults.
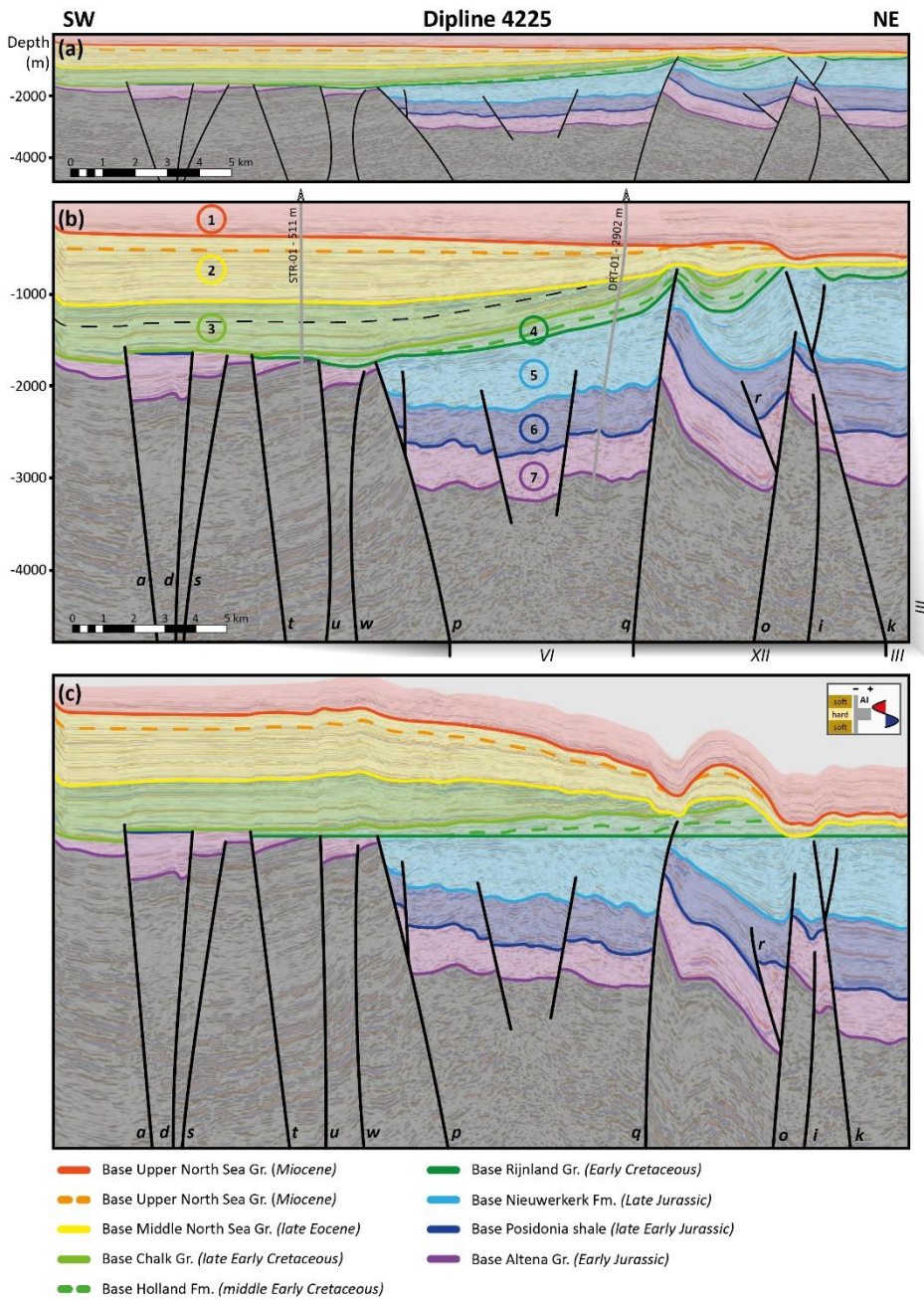
Figure 5: Dipline 4225 displayed with three different scales; (a): 1:1 scale, displayed with the interpreted horizons, megasequences and faults; (b): 1:3 scale, displayed with the interpreted horizons, megasequences and faults, together with projected wells and their distance to the seismic line, and the unconformity within megasequence 3 (marked by the black dotted line). Below the section, the sub-basins and highs are numbered as in Figure 7 ((VI): Dordrecht Graben, (XII): Ridderkerk Graben, (III): Zoetermeer Graben); (c): the 1:3 scaled section flattened for the base of the Rijnland Group, displayed with the interpreted horizons, megasequences and faults.

Legend:
- Base Upper North Sea Gr. (*Miocene*)
- Base Upper North Sea Gr. (*Miocene*)
- Base Middle North Sea Gr. (*late Eocene*)
- Base Chalk Gr. (*late Early Cretaceous*)
- Base Holland Fm. (*middle Early Cretaceous*)
- Base Rijnland Gr. (*Early Cretaceous*)
- Base Nieuwerkerk Fm. (*Late Jurassic*)
- Base Posidonia shale (*late Early Jurassic*)
- Base Altena Gr. (*Early Jurassic*)

295

300

4.1.3 Dipline 4225

Dipline 4225 (Fig. 5) is located 16 km SE of dipline 3410 and it does not crosscut any wells of an hydrocarbon field or geothermal energy projects (Fig. 1c). From the projected wells (Fig. 5b), STR-01 resulted in oil and gas shows, while well DRT-01 was dry.

Megasequence 1 shows subhorizontal reflectors, floored by a major erosional surface. Below, megasequence 2 shows gently dipping reflectors, that are truncated towards the NE by the basal unconformity of megasequence 1. Towards the SW, the underlying megasequence 3 shows parallel reflectors, which are also parallel to those of megasequence 2 , while in the underlying Dordrecht and Ridderkerk grabens (structures VI and XII, Fig. 5b), an unconformity separates these two megasequences. The intra-sequence unconformity, which is also observed in diplines 2610 and 3410, separates the uppermost and lowermost parts of megasequence 3 in dipline 4225 (black dashed line in Fig. 5b). In the SW, megasequence 3 is affected by faults. Megasequence 4 thins from 200 to 0 m towards the SW and is affected by a syncline and fault-cored anticlines towards the NE, leading to erosion and the unconformable deposition of megasequence 2 on top. Faults *a* and *q* crosscut the upper part of megasequence 4. Megasequence 5 is only present towards the NE portion of the section. Like in the previous diplines, megasequence 5 is affected by faults *p*, *q*, *o*, *i* and *k*, and shows abrupt thickness changes ranging from 1000 to 0 m, even better visible on the flattened section (Fig. 5c). In the Ridderkerk Graben (structure XII, Fig. 5b), megasequence 5 has a maximum thickness of 750 m and forms a fault-bounded half-graben. The underlying megasequence 6 has an average thickness of 500 m and includes parallel reflectors. Thickness variations are restricted to the NE part of the section in the Ridderkerk and Zoetermeer grabens (structures XII and III, Fig. 5b), where megasequence 6 is 100 to 750 m thick, due to erosion atop former structural highs. Megasequence 7 includes parallel layers, showing locally slight thickness changes, well evident in the Ridderkerk and Zoetermeer grabens, where it is 300 to 800 m thick.

Twelve major faults are recognized in this seismic section, comprising both normal and partially (in the lowermost tracts) inverted faults. Faults *a*, *d*, *i* and *k* are also recognized in dipline 2610, while faults *d*, *o*, *i* and *k* also appear in dipline 3410. Megasequences 5 and 7 are affected by all the displayed faults, from which faults *a*, *p*, *q*, *o* and *k* show evidence of positive inversion. Megasequence 4 is cut by faults *p* and *q*, and megasequences 1 and 2 are un-faulted. Unlike dipline 2610 and 3410, were also megasequence 3 remains un-faulted, here megasequence 3 is affected by the positively inverted fault *a*. This contrasts with observations performed in section 2610, where fault *a* doesn't show inversion and is capped by megasequence 4. The SW-side of fault *p* marks the edge of the WNB, with faults *a*, *d*, *s*, *t*, *u* and *w* forming horst and graben structures. The infill of the horst and graben structures includes megasequence 7 and a 50 m thick megasequence 6, which are capped by either megasequence 3 or 4. Faults *p* and *q* bound the Dordrecht Graben (structure VI, Fig. 5b) that shows some internal normal faulting. Faults *p* and *q* show positive inversion in their uppermost segments, evidenced by an antithetic fault in the upper part of fault *p* and the development of a fault-cored anticline in megasequence 4 atop fault *q*. Towards the NE, faults *q* and *k* bound the Ridderkerk Graben (structure XII, Fig. 5b). Faults *o* and *k* bound a former structural high underlying this graben. As observed in section 3410, the inversion of fault *o* resulted in the development of an antithetic fault, here called fault *r*, which

335 affects megasequences 6 and 7 in dipline 4225. Inside the former structural high, fault *i* is normally displacing megasequence 7. This contrasts with observations in seismic lines 2610 and 3410, where fault *i* shows positive inversion in the upper segment. Towards the NE, like in section 3410, fault *k* bounds the Zoetermeer Graben (structure III, Fig. 5b). In contrast with observations performed in seismic lines 2610 and 3410, where fault *k* does not show evidence of inversion, an antithetic fault formed in the upper segment as a result of reverse offset in seismic line 4225.
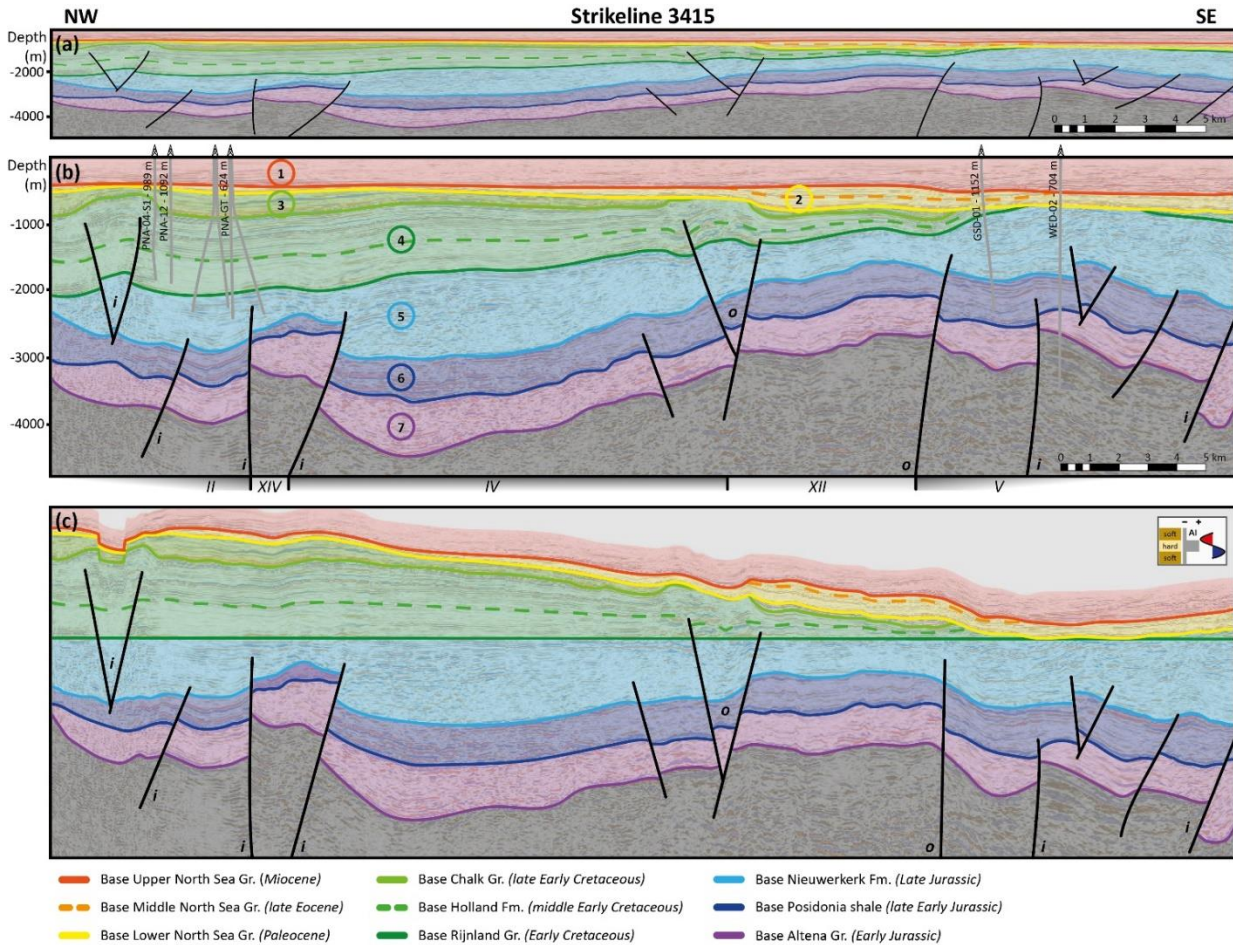
340

Figure 6: Strikeline 3415 displayed with three different scales; (a): 1:1 scale, displayed with the interpreted horizons, megasequences and faults; (b): 1:3 scale, displayed with the interpreted horizons, megasequences, faults and projected wells with their distance to the seismic line. The strikeline intersects fault *i* several times, wherefore the fault can be recognized multiple times. Below the section, the sub-basins and highs are numbered as in Figure 7 ((II): Voorburg Graben, (XIV): Lansingerland High, (IV): Pijnacker Graben,
345 **(XII): Ridderkerk Graben, (V): Biesbosch Graben); (c): the 1:3 scaled section flattened for the base of the Rijnland Group, displayed with the interpreted horizons, megasequences and faults.**

4.1.4 Strikeline 3415

Strikeline 3415 (Fig. 6) runs perpendicular to the previously described lines, crossing the NE part of the study area, the Werkendam abandoned oil field (WED-02) and the undeveloped Werkendam-Diep gas field. Nearby is the dry GSD-01 well, the Pijnacker (PNA-04-S1 & PNA-12) abandoned oil field and the producing geothermal energy project (PNA-GT wells) (hydrocarbon fields 5, 13 and 14, Fig. 1c).

Megasequence 1 is characterised by subhorizontal reflectors and is underlain by an erosional surface. Megasequence 2 shows thickness variations ranging from 50 to 350 m, associated with uplift and erosion. Reflectors within megasequence 3 lap onto the limbs of anticlines cored by faults *i* and *o*. Megasequence 2 toplaps megasequence 3, which wedges out from 400 to 0 m towards the SE. The base of megasequence 2 represents and erosional surface that truncates open anticlines and synclines, showing erosion of megasequences 3, 4 and 5 at the hinges of the anticlines. Megasequence 4 includes parallel reflectors, has an average thickness of 1100 m in the Voorburg and Pijnacker grabens and the Lansingerland High (structures II, IV and XIV), and thins to 0 m along the Ridderkerk and the Biesbosch grabens (structures XII and V) towards the SE. The underlying megasequence 5 displays thickness variations ranging from 500 to 1300 m across short distances. No clear boundary faults can be identified in this line for the growth-structures observed in megasequence 4, corroborating the idea that the major faults are oriented at low angle to this seismic section. Also, megasequence 5 includes parallel reflectors and chaotic seismic facies. Megasequence 6 does not show remarkable thickness variations, having an average thickness of 550 m. The lowermost megasequence 7 shows some slight changes in thickness ranging from 400-900 m.

As section 3415 crosscuts the main faults at a low angle, relatively mildly deformation is observed. Fault *i* is parallel to and can be interpreted several times along the section, suggesting that it extends throughout the whole 3D cube and bends along the section towards the SE. Minor folding is observed in megasequence 4 related to fault *i*, but no distinct inversion structures are recognized. In the middle of the section, fault *o* bounds the Ridderkerk Graben (structure XII, Fig. 6b), and shows a related second-order pop-up structure on the NW-boundary of this horst, which is the same pop-up structure as observed along fault *o* in section 3410. Except for the second-order pop-up structures related to faults *i* and *o* that are capped by megasequence 3, all faults are sealed by megasequence 4.

4.2 Thickness maps

Megasequence 1 represents the youngest unit and is bounded upwards by the seafloor, therefore the depth map of its base is representative of its thickness (Fig. 7a). Figures 7b to g display the thickness maps of megasequences 2 to 7. Overall, megasequence 1 shows a constant thickness of about 400 m, but it thickens up to 650 m towards the E. This is related with the only fault crosscutting this megasequence, which is an extension of fault *k* (dipline 4225, Fig. 5b). Megasequence 2 thins from 800 to 0 m towards the NE (Fig. 7b), due to the uplift and erosion that led to the development of the overlying erosional surface, as observed in all seismic lines (Figs. 3-6). Within megasequence 2, we also observe the occurrence of narrow NNW-SSE and NW-SE elongated areas showing an increase in sediment thickness from 200 to 500 m. In the three seismic diplines

(Figs. 3-5), inverted faults cut megasequence 3, resulting in thickness variations of up to 800 m along elongated areas that
380   correspond to folds (Fig. 7c). The overall NE-ward thinning from up to 800 to 0 m was related to erosion, due to basin inversion. The erosional surface at the base of megasequence 1 that is observed on all seismic sections (Figs. 3-6), correlates with NNW-SSE and (mostly) NW-SE elongated areas where the thickness is reduced to 0 m for both megasequences 2 and 3.

In contrast to the thickness variations of megasequence 3, megasequence 4 displays an overall thinning from 1500 to 0 m towards the S, with no localised areas of maximum or minimum thicknesses (Fig. 7d). Megasequence 5 (the main geothermal
385   target interval) is characterised by an overall thickness increase from 0 to 1200 m towards the NE (Fig. 7e). NW-SE and NNW-SSE oriented faults bound areas of increased and reduced thicknesses that are mostly lozenge-shaped. Towards the S, the thickness of megasequence 5 is about 0 m, due to erosion and/or non-deposition. Sub-basins filled by megasequence 5 are asymmetric, as evidenced by the abrupt thickness changes ranging from 400 to 1400 m that are observed towards the NE. This contrasts with the progressive thinning from 600 to 0 m towards the SW. Such an observation is suggestive of a first order
390   architecture composed of half-grabens bounded by SW-dipping master faults.

The interpretation of the thickness maps of megasequences 6 and 7 is more complex, as these megasequences experienced multiple tectonic events that caused faulting, folding and erosion. These thickness maps show the effects of erosion during the deposition of megasequence 5, e.g., in the horst structure between faults *b* and *c* in section 2610 (Fig. 3). This effect is seen in the map as NNW-SSE oriented ribbons of reduced thickness (roughly up to 1000 m thinner than the surrounding topography),
395   resembling horst structures. If we remove the effect of those ribbons from the thickness maps of megasequences 6 and 7, and we rely on the occurrence of growth geometries (such as the growth wedge observed in megasequence 7 in the Voorburg Graben, structure II, close to fault *j*, Fig. 3b), we can make some observations regarding the thickness variations. Megasequence 6 is 0 to 1100 m thick (Fig. 7f). None of the thicker areas (between 600 and 1100 m) show growth wedge geometries, suggesting that thickness variations resulted from later erosion rather than to syn-sedimentary creation of accommodation space.
400   Megasequence 7 describes NW-SE elongated grabens/half-grabens where thicknesses increases abruptly from 400 to 1200 m (Fig. 7g). The infill consists of asymmetrically wedge-shaped growth strata, which are separated by horst structures. The Lansingerland High is an outstanding example in the northern corner of the map. This structure is a 20 km long NW-SE elongated horst (structure XIV, Figs. 4 and 7h) that shows a 1400 m thick sedimentary succession bounded by two depocenters. In the depocenters and the horst, the thickness of megasequence 6 remains a stable 500 m. This contrasts with megasequence
405   5 and 7, where changes in thickness are recognized: from a maximum of 1000 m in the depocenters to 400 m on the horst for megasequence 5, and from a maximum of 800 m in the depocenters to 500 m on the horst for megasequence 7.
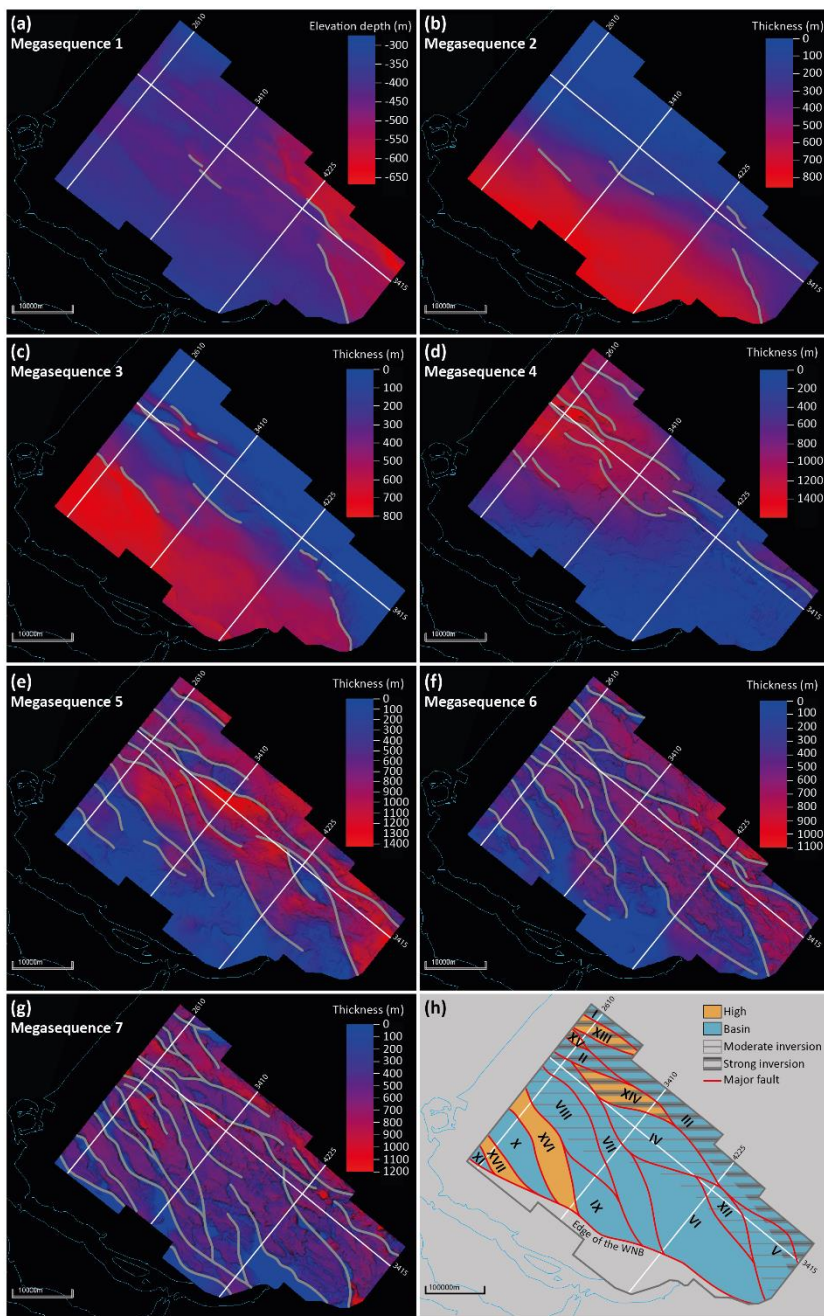
Figure 7: (a): Depth map of megasequence 1, with present faults displayed in grey; (b-g): thickness maps of megasequences 2–7 with present faults displayed in grey; (h): Simplified map showing the structural elements formed as consequence of the first and second rifting episodes, together with a qualitative estimation of the degree of inversion. The seismic section displayed in figures 3-6 are displayed, together with the different highs and basins, which are numbered and named; (I): Waddinxveen Graben, (II): Voorburg Graben, (III): Zoetermeer Graben, (IV): Pijnacker Graben, (V): Biesbosch Graben, (VI): Dordrecht Graben, (VII): Rijswijk Graben, (VIII): Westland Graben, (IX): Spijkenisse Graben, (X): Maasland Graben, (XI): Voorne Graben, (XII): Ridderkerk Graben, (XIII): Moerkapelle High, (XIV): Lansingerland High, (XV): Zoetermeer High, (XVI): De Lier High, (XVII): Hoek van Holland High.

5 Discussion

5.1 Tectonic evolution

The interpretation of the L3NAM2012AR seismic 3D cube has allowed us to define seven megasequences, including sediments spanning in age from Jurassic to Present times. Megasequences are delimited either by unconformities (base of megasequences 1, 2, 4 and 5), or by the transition from unconformity (e.g. growth geometries, stratigraphic fanning/expansion-tapering, convergent reflectors) to correlative conformity (e.g. parallel geometries). Intra-formational unconformities are also observed. However, in the framework of a reconstruction of the subsurface, only the main seismo-stratigraphic units are defined. Based on our observations, the evolution of the studied portion of the WNB from the Jurassic onwards can be assessed.

The first observed tectonic period can be dated to the Early Jurassic, which is the biostratigraphic age of the sedimentary rocks of megasequence 7. NW-SE elongated regions of reduced or thick sediments showing thickness variations of up to 800 m (Fig. 7g) are interpreted as Early to Middle Jurassic fault-bounded horst and graben structures, respectively. Growth geometries within this megasequence are observed, like the structures observed in the half-graben in the Voorburg Graben (structure II, associated with fault *j*, Fig. 3b). Coherently, megasequence 7 is interpreted as a syn-rift sequence, with the syn-rift infill thickening roughly 600 m towards the NE (Fig. 7g). Regionally, this rifting stage is synchronous with the final stage of the first rifting event that has shaped the North Sea Rift system (e.g. Fossen et al., 2021). This rifting event seems to overlap with the regionally recognized Early Kimmerian tectonics (Fig. 2) (Geluk and Röhling, 1997; Duin et al., 2006). The overlying megasequence 6 displays areas of slight thickness variations of up to 400 m (Fig. 7f). Erosion and non-deposition caused these variations, such as the Hoek van Holland, De Lier and Zoetermeer former structural highs (structures XVII, XVI and XV, Fig. 3b). No growth geometries are observed within megasequence 6, therefore being interpreted as a post-rift unit. Overall, both megasequence 6 and 7 display a slight NE-ward thickening (Figs. 7f and g), with the thickening direction being perpendicular to the direction of the main normal faults that were active during the Early Jurassic rifting stage. According to the widely recognised features in rift systems (e.g. Franke, 2013; Peron-Pinvidic et al., 2019), we interpret the creation of accommodation space synchronously with deposition of megasequence 7 and the overlying megasequence 6 as the post-rift passive infill. Since the timing of deposition of megasequence 6 corresponds to the inception of the thermal North Sea Rift Dome underneath the central North Sea (van Wijhe, 1987; Ziegler, 1992), an alternative hypothesis could be that thinning of megasequence 6 is somehow related with this lithospheric-scale bulging process. Given that the centre of the dome was located further to the N (between NW Scotland and SE Norway) (Ziegler, 1992; Wong et al., 2007), N-ward thinning of megasequence 6 should be observed, which is not the case. Yet, it should be noted that later structural deformation events could have overprinted subtle effects related to the North Sea Rift Dome. Still, the absence of N-ward thinning makes us to discard the hypothesis of doming causing large impact on the depositional pattern of megasequence 6.

Deposition of the overlying megasequence 5 started in the Late Jurassic, during a second pulse of extensional faulting. The observed local unconformities within megasequence 5 suggest that faulting happened in several pulses. This stage is coeval with the second phase of rifting observed in the North Sea, further to the N (e.g. Færseth, 1996), which induced crustal

450 extension, known as the Late Kimmerian tectonics (van Wijhe, 1987; Ziegler, 1992; de Jager, 1996; Racero-Baena and Drake, 1996; van Balen et al., 2000). In the WNB, this extensional phase is simultaneous with igneous activity (Sissingh, 2004), a characteristic of continental rifting (e.g. Franke, 2013; Gouiza and Paton, 2019). We observe that the upper portion of megasequence 5 postdates all the normal faults (excluding those showing evidence of reverse reactivation). Similarly to megasequences 7 and 6, megasequence 5 thickens towards the NE (Fig. 7e), suggesting that these megasequences form part

455 of the same multiphase rift system. Several syn-depositional wedges, mostly describing half-grabens, are observed in megasequence 5, such as those associated with faults *h*, *o* and *i* (Fig. 4). The various sub-basins active during this second extensional pulse are lozenge-shaped, bounded by NW-SE and NNW-SSE striking faults (Fig. 7e). The Westland, Pijnacker, Dordrecht and Biesbosch grabens are good examples of this (structures VIII, IV, VI and V, Fig. 7h). Their 'zigzag' arrangement of faults is a typical feature when pre-existing faults occur (e.g., Henstra et al., 2019). Many horst and grabens active during

460 this second rifting phase retrace structures developed during the first rifting stage, such as the ones seen in the NW part of the study area (e.g. the Westland and Pijnacker grabens, structures VIII and IV, Fig. 7h). Our observations show that during the first rifting stage the structures were NW-SE oriented. This allowes us to infer that during the second rifting phase, these NW-SE striking structures were reactivated and that the NNW-SSE striking normal faults were formed. Such an inference is coherent with natural examples and analogue models of multiphase rift systems, where it is commonly observed that oblique

465 inherited structures can be reactivated synchronously with the formation of new faults oriented perpendicular to the stretching direction (e.g. McClay and White, 1995; Mart and Dauteuil, 2000; Henza et al., 2010; Brune et al., 2014; Naliboff and Buiter, 2015; Zwaan et al., 2016; Zwaan and Schreurs, 2017; Cadenas et al., 2020). An alternative hypothesis is that the lozenge-shaped structures are pull-apart basins or ridges associated with transtensive/transpressive faults. We discard this hypothesis for the studied area, as we do not observe the diagnostic features of wrench tectonics, such as positive/negative flowers, branch

470 faults, restraining/releasing bends, antithetic faults and/or strike-slip duplexes (e.g. Riedel, 1929; Wilcox et al., 1973; Harding, 1974; Aydin and Nur, 1982; Sanderson and Marchini, 1984; Woodcock and Fischer, 1986; Sylvester, 1988; among others) in the L3NAM2012AR 3D seismic cube.

After diminishing the second period of rift-related Jurassic crustal extensions (e.g. Ziegler, 1992), the WNB entered a post-rift phase in the Early Cretaceous (van Wijhe, 1987). None of the observed extensional faults were active at that time. Post-rift

475 infill of the WNB is well represented by megasequence 4 on the flattened displays of diplines 2610, 3410 and 4225 (Figs. 3c, 4c and 5c) and on the thickness map, showing a NW-SE elongated, 20 to 40 km wide, post-rift basin where the thickness of megasequence 4 increases with roughly 1000 m (Fig. 7d). Such a broad basin does not overlap the syn-rift grabens and, therefore, it likely relates to large-scale sagging rather than to the simple passive infill of the previously developed half-grabens. On top of the post-rift megasequence 4, the Lower Cretaceous megasequence 3 was deposited during a shortening stage. Strata

480 within this megasequence describe growth geometries and buttressing-related structures in the hanging-wall of positively inverted normal faults (e.g. associated with faults *e*, *h* and *i* in Fig. 3 and fault *a* in Fig. 5). This Late Cretaceous period of inversion likely corresponds to the Late Cretaceous Subhercynian inversion phase (Fig. 2) (e.g. Ziegler, 1992; van Wijhe, 1987; de Jager 2003, Worum and Michon, 2005), caused by the convergence between Africa and Europa (Kley and Voigt,

2008). During this stage, the NW-SE and NNW-SSE fault systems were inverted or deformed due to buttressing. Yet, we were not able to individuate newly formed reverse faults, which are a requirement to constrain the shortening direction. While the NE-section of the WNB was inverted and uplifted, its SW-flank underwent subsidence and developed as a marginal basin, referred to as the Voorne Trough (Deckers, 2015), where megasequence 3 thickens from 0 to 800 m towards the SW (Fig. 7c). The upper portion of megasequence 3 may represent post-inversion succession. In fact, a local unconformity divides the upper from the central and lower portions of this megasequence (Figs. 3-5). This is consistent with regional constraints, indicating that due to a decrease in the convergence rate between Africa and Europa (Rosenbaum et al., 2002), the Subhercynian inversion ceased after the Campanian (de Jager, 2003), whereafter deposition of the chalk deposits of megasequence 3 continued till the end of the Late Cretaceous (van Balen et al., 2000; van der Voet et al., 2019).

Megasequence 2 is floored by a regional unconformity and no growth wedge geometries are observed in this megasequence, suggesting that the gentle folding observed at its base is associated with compaction of the underlying sediments and/or the passive infill/draping of a paleo-topography. Both the syn-inversion megasequence 3 and the post-inversion megasequence 2 are wedging out toward the NE (Figs. 7b and 7c), indicating that uplift of the NE sector of the study area started during faults' inversion. Evidenced by the SW-tilting of the erosional unconformity separating the two megasequences, the uplift continued during the deposition of megasequence 2. The erosional unconformity at the base of megasequence 2 likely corresponds to the timing of the Laramide uplift that peaked during the Middle Paleocene (Deckers, 2015), which may be related to a significant drop in global sea-level (Haq et al., 1987), along with a contribution from dynamic topography due to mantle flow (Kley, 2018; Voigt et al., 2021). The Laramide tectonic phase may have been responsible for the uplift in the area of the WNB (Deckers and van der Voet, 2018; Kley, 2018). The erosional unconformity at the top of megasequence 2, instead, reflects a broad basin uplift (de Jager, 2003), likely initiated during the Alpine Orogeny (Worum and Michon, 2005). Lastly, the depth map of the base of megasequence 1 displays two large plateaus (Fig. 7a), separated by an ENE-dipping fault formed during the second extensional phase and reactivated during the Miocene.

5.2 Implications for geothermal systems

The WNB harbours well developed geothermal reservoir rocks and is covered by a good data-collection, inherited from former hydrocarbon exploration (e.g. Willems et al., 2020). Presently, the most exploited geothermal reservoir units are the Late Jurassic Nieuwerkerk Formation (megasequence 5; second syn-rift) and, subordinately, the Cretaceous sandstones (megasequence 4, post-rift and pre-inversion). An additional reservoir is represented by the Triassic sandstones, which occur below the Altena Group and have not been mapped in this work. Although the first characterised rifting period is Early Jurassic in age, the kinematics and type of rift-related structures may have been similar during both the Jurassic and Triassic rifting periods. The Early Jurassic rifting episode can be linked to the regional Early Kimmerian tectonic phase, which started during the early Late Triassic (e.g. van Wijhe, 1987; Ziegler, 1992; Geluk and Röhling, 1997, Fig. 2) and reactivated basement faults (Kortekaas et al., 2018), wherefore the Early Jurassic rift might be a continuation from Triassic tectonics. The Triassic sandstones have a reduced reservoir quality (Boersma et al., 2020). The fault k does not show signs of reactivation during

inversion (Fig. 3), suggesting that the Zoetermeer High (structure XV in figures 3b and 7h) may have been relatively stable throughout the evolution of the WNB. Therefore, the Triassic reservoir might be less fractured. In the Zoetermeer High, it shows shallower burial conditions than in the surrounding grabens, and its quality as geothermal reservoir may be better.
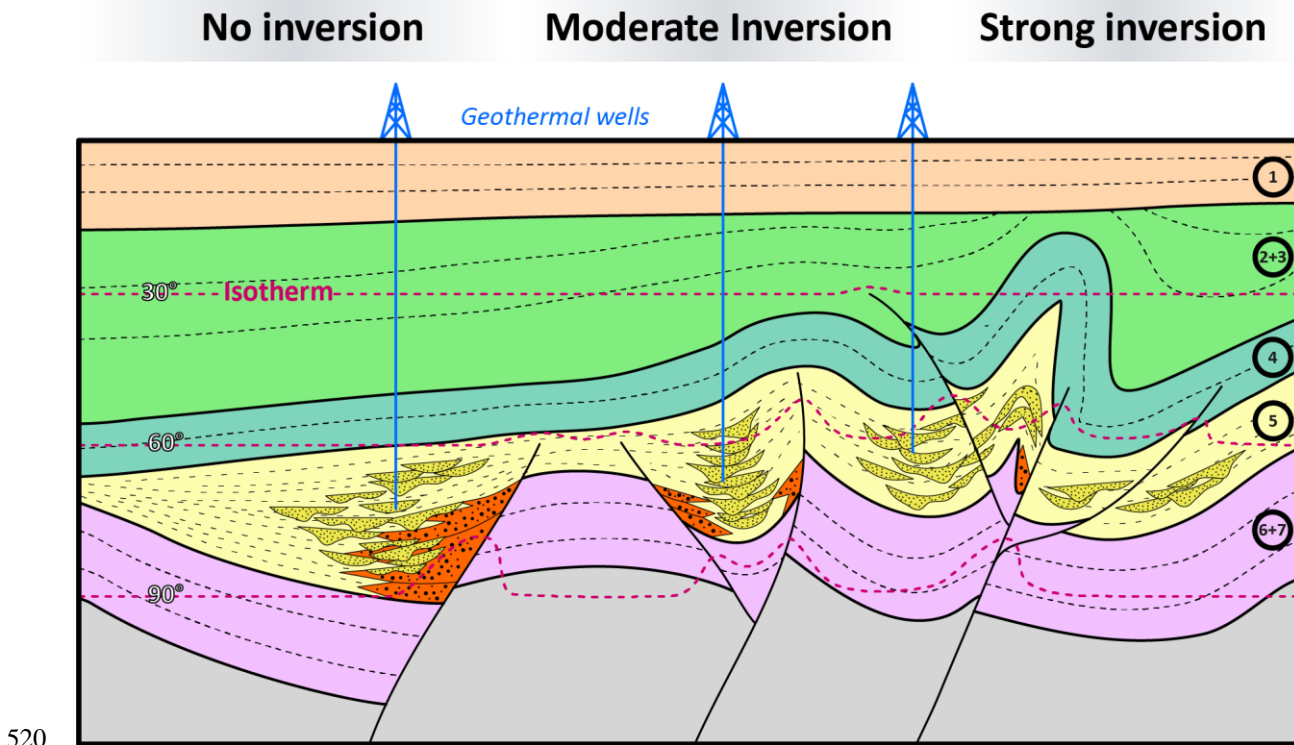
Figure 8: Simplified cartoon, showing the geothermal play of a fluvial-deltaic reservoir in an inverted rift basin. The expected best spots for geothermal exploration are the central portions of the half-grabens, where the fluvial sands (yellow dotted material) are present, the geothermal gradients are highest, and the interference from foot-wall erosion (orange dotted material) is minor. The isotherms are based on a geotherm of 31°C km⁻¹ (Bonté et al., 2012). The sketched layers are based on the interpreted megasequences on this study, indicated in the circles on the right side.

Among the two Jurassic-Cretaceous reservoirs, the Jurassic Nieuwerkerk Formation is the most promising. It facilitates a deeper reservoir (spanning in depth from 0.5 km to 3 km) and, given the geothermal gradient of the area (Fig. 8, 31°C km⁻¹; Bonté et al., 2012), it likely offers temperatures up to 90°C, which is suitable for low enthalpy geothermal systems. Instead, temperatures for the Cretaceous sandstones of the Rijnland Group (spanning in depth from 0.5 km to 2 km) probably do not exceed 60°C. The Nieuwerkerk Formation (megasequence 5) was deposited during the second rifting event in the Late Jurassic and the multi-phase extension led to the development of a compartmentalised reservoir, made up of lozenge-shaped sub-basins. Given the fluvial nature of the Nieuwerkerk Formation (e.g. Willems et al., 2017c; Vondrak et al., 2018; Willems et al., 2020), the lateral and vertical compartmentalization of sands and shales is a characteristic that must be taken into account for reservoir's geothermal exploration.

The geothermal play of such a fluvial-deltaic reservoir in an inverted rift basin is illustrated in Figure 8, where normal faults, positively inverted normal faults, half-grabens, geotherms and sweet spots are outlined. In rift systems involving continental

to coastal clastic syn-tectonic sedimentation, it is well known that the more coarse-grained facies are located close to the faults and along the axis of grabens and half-grabens (e.g., Gawthorpe and Leeder, 2000). In agreement, we expect fluvial channels and other coarse grained sediments in the core of half-grabens or in the inner limbs close to master faults. Furthermore, close to the master fault, foot-wall erosion and related hanging-wall degradation complexes drive to the development of a wide spectrum of heterogeneous sedimentary facies, possibly interfingered with the targeted reservoir rock. In contrast to petroleum systems, in which structural highs are the preferential targets for hydrocarbon exploration (hydrocarbons are lighter than water) (e.g. Bjørlykke, 2010), half-grabens are the most suitable sites for geothermal exploration. Indeed, half-grabens are deeper, thus ensuring higher temperatures than adjacent limbs and structural highs. All these characteristics allow us to individuate the core of half-grabens, i.e. syn-tectonic intervals in the core of half-grabens, as preferential sites for geothermal exploration. These areas have greater chances of finding hot and thick fluvial sand packages with a higher nett to gross ratio.

Such a simple template is modified during faults' reactivation and buttressing associated with inversion tectonics. Inversion can produce (1) the uplift of the former structural-stratigraphic reservoirs, i.e. the half-grabens, with the consequent decrease of water temperatures and, eventually, (2) fracturing of the reservoirs by second order faults and brecciation and breaching of the reservoir due to an increase in the inversion (e.g. Tari et al., 2020).

Given the template illustrated in Figure 8 and assuming that the most suitable areas for geothermal exploration are the central portions of the half-grabens, synclinal traps in half-grabens associated with highly inverted faults are more likely to be breached by faults during inversion tectonics. The effects of a secondary fracturing period due to inversion tectonics can be beneficial in terms of permeability (e.g. Fisher and Knipe, 2001). Instead, the consequences of breaching a geothermal reservoir due to inversion tectonics are less clear. In hydrocarbon reservoirs, indeed, breaching of the anticlinal traps has a clear negative effect (i.e. leakage of the hydrocarbons), while the consequences of breaching synclinal traps in geothermal systems are not yet fully understood. In order to de-risk geothermal exploitation, we therefore advise to choose half-grabens associated with either non-inverted or moderately inverted normal faults. By combining these findings, we can identify areas of interest for geothermal exploitation. Examples of such areas are the central portions of the Pijnacker, Rijswijk and Westland grabens (structures IV, VII and VIII, Figs. 4, 7e and 7h). These grabens contain a 1 to 1,4 km thick megasequence 5 (Nieuwerkerk Formation) with no to moderate inversion. The deepest portions of these grabens are located away from the master faults, preventing the interference by material originating from foot-wall erosion (e.g. the Pijnacker Graben, structure IV, Fig. 4). The central parts of these grabens are 2 to 3 km deep (Fig. 4b), with expected temperatures between 60°C and 90°C for the sand bodies (based on a geotherm of 31°C km^{-1}; Bonté et al., 2012). In such areas, additional work is required to assess the fluvial reservoir architecture (Willems et al., 2017a) in more detail and properly locate injection and recovery wells (i.e. geothermal doublets) within coarse grained sediments.

6 Conclusion

The seismic interpretation of the recently released L3NAM2012AR 3D depth-migrated seismic cube allowed for the identification of seven megasequences, three main fault trends, and the mapping of horst and grabens and major bounding faults in the WNB. This helps to better understand the overall structure of the sedimentary infill, and the tectonic evolution of the major faults and the syn-rift infill, which hosts the main geothermal reservoir.

- Faults affecting the Mesozoic sequence of the WNB can be arranged in three main trends. The first fault trend comprises NW-SE striking extensional faults that cut the Early Jurassic syn-tectonic megasequence 7. The second fault trend includes NNW-SSE striking extensional faults and reactivated faults of the first fault trend, affecting megasequences 7 and 6, and the Late Jurassic syn-tectonic megasequence 5. The third trend comprises reversely reactivated NW-SE and NNW-SSE oriented faults from the first and second fault trend, that affect megasequences 4 to 7, and the Late Cretaceous syn-tectonic megasequence 3.

- Fault kinematics and the age of syn-kinematic units enable the definition of seven main tectonic phases; (1): a first NE-SW oriented Early Jurassic rifting phase; (2): a Middle Jurassic post-rift phase; (3): a second WSW-ENE oriented Late Jurassic rifting phase, partly controlled by the Early Jurassic rifting phase; (4): an Early Cretaceous post-rift sag phase; (5): a Late Cretaceous orogenic phase, which led to the inversion of pre-existing extensional faults; (6): a regional Paleocene to Oligocene basin uplift; (7): a minor Miocene orogenic phase of fault reactivation.

- The lozenge-shaped sub-basins filled by megasequence 5 suggest that the Jurassic multi-phase rifting led to compartmentalization of the main geothermal target in the WNB, corresponding to the Late Jurassic fluvial-deltaic Nieuwerkerk Formation.

- The presence of heterogeneous seismic facies within the detric syn-rift sediments of the Nieuwerkerk Formation in the half-graben structures suggests that channel sands are likely present in their deepest, central portions. The highest temperatures and minimal interference by foot-wall erosion and residue hydrocarbons are expected in these areas.

- The increase of Late Cretaceous inversion raises the risks for geothermal exploration. Reactivation of extensional faults could have caused breaching of the reservoir and uplift of the targeted half-grabens, hence decreasing the temperature. Therefore, only non to moderately inverted areas should be considered for geothermal exploration.

Hence, we conclude that for a fluvial-deltaic syn-rift reservoir rock in a geothermal play resulting from a multi-phase rift setting that undergoes a subsequent basin inversion, the best spots for geothermal exploration can be found in the central portions of non to moderately inverted half-grabens.

Supplementary materials

The supplementary materials include:

- a list of used wells with their coordinates, drilling result and whether a LAS-file is available,

- links to the public datasets with a description of how to download them,
- a folder with TIFF-files of the uninterpreted seismic lines together with some information about the L3NAM2012AR 3D seismic cube and how to download it.

Author contribution

AW, corresponding author, conceptualisation, data acquisition and processing, seismic interpretation, figures and manuscript drafting/editing; KO, interpretation assistance, figures and manuscript drafting/editing; FV, data acquisition, manuscript drafting/editing; CL, data acquisition, interpretation assistance, manuscript drafting/editing; GB, manuscript drafting/editing; JA, manuscript drafting/editing; ST, conceptualisation, data processing, interpretation assistance, figures and manuscript drafting/editing.

Competing interests

KO and ST are member of the editorial board of Solid Earth.

Acknowledgments

This work was funded by a full PhD scholarship (PON-REACTEU) from the Ministry of University and Research of Italy. PanTerra Geoconsultants B.V. is thanked for funding this project and for providing in-house expertise that greatly improved the quality of the research. We thank Schlumberger for providing access to Petrel Software (version 2020.3). David Iacopini is thanked for his help that greatly improved the quality of the work. We thank an anonymous reviewer and Connor O'Sullivan for their detailed and constructive comments and suggestions, which allowed us to improve the manuscript. The handling editor Patricia Cadenas Martínez and the executive editor Susanne Buiter are also thanked for guiding the review process.

References

van Adrichem Boogaert, H. A. and Kouwe, W. P. F.: Stratigraphic nomenclature of the Netherlands, revision and update by RGD and NOGEPA, 1993.

Aydin, A. and Nur, A.: Evolution of pull-apart basins and their scale independence, Tectonics, 1, 91–105, https://doi.org/10.1029/TC001i001p00091, 1982.

van Balen, R. T., van Bergen, F., de Leeuw, C., Pagnier, H., Simmelink, H., van Wees, J. D., and Verweij, J. M.: Modelling the hydrocarbon generation and migration in the West Netherlands Basin, the Netherlands, Netherlands Journal of Geosciences - Geologie en Mijnbouw, 79, 29–44, https://doi.org/10.1017/S0016774600021557, 2000.

Bjørlykke, K. (Ed.): Petroleum Geoscience: From sedimentary environments to rock physics, Springer Science and Business Media, Heidelberg, Germany, 662 pp., ISBN 978-3-642-34131-1, 2010.

Boersma, Q. D., Bruna, P. O., de Hoop, S., Vinci, F., Moradi Tehrani, A., and Bertotti, G.: The impact of natural fractures on heat extraction from tight Triassic sandstones in the West Netherlands Basin: a case study combining well, seismic and numerical data, Netherlands Journal of Geosciences, 100, e6, https://doi.org/10.1017/njg.2020.21, 2021.

Bonté, D., van Wees, J. D., and Verweij, J. M.: Subsurface temperature of the onshore Netherlands: new temperature dataset and modelling, Netherlands Journal of Geosciences - Geologie en Mijnbouw, 91, 491–515, https://doi.org/10.1017/S0016774600000354, 2012.

Brune, S., Heine, C., Pérez-Gussinyé, M., and Sobolev, S. V.: Rift migration explains continental margin asymmetry and crustal hyper-extension, Nature Communications, 5, 4014, https://doi.org/10.1038/ncomms5014, 2014.

Cadenas, P., Manatschal, G., and Fernández-Viejo, G.: Unravelling the architecture and evolution of the inverted multi-stage North Iberian-Bay of Biscay rift, Gondwana Research, 88, 67-87, https://doi.org/10.1016/j.gr.2020.06.026, 2020.

Carapezza, M. L., Chiappini, M., Nicolosi, I., Pizzino, L., Ranaldi, M., Tarchini, L., de Simone, G., Ricchetti, N., and Barberi, F.: Assessment of a low-enthalpy geothermal resource and evaluation of the natural CO2 output in the Tor di Quinto area (Rome city, Italy), Geothermics, 99, 102298, https://doi.org/10.1016/j.geothermics.2021.102298, 2022.

Crooijmans, R. A., Willems, C. J. L., Nick, H. M., and Bruhn, D. F.: The influence of facies heterogeneity on the doublet performance in low-enthalpy geothermal sedimentary reservoirs, Geothermics, 64, 209–219, https://doi.org/10.1016/j.geothermics.2016.06.004, 2016.

Deckers, J.: The Paleocene stratigraphic records in the Central Netherlands and close surrounding basins: Highlighting the different responses to a late Danian change in stress regime within the Central European Basin System, Tectonophysics, 659, 102–108, https://doi.org/10.1016/j.tecto.2015.07.031, 2015.

Deckers, J. and van der Voet, E.: A review on the structural styles of deformation during Late Cretaceous and Paleocene tectonic phases in the southern North Sea area, J Geodyn, 115, 1–9, https://doi.org/10.1016/j.jog.2018.01.005, 2018.

660   DeVault, B. and Jeremiah, J.: Tectonostratigraphy of the Nieuwerkerk Formation (Delfland subgroup), West Netherlands Basin, AAPG bulletin, 86, 1679-1707, https://doi.org/10.1306/61EEDD50-173E-11D7-8645000102C1865D, 2002.

Duin, E. J. T., Doornenbal, J. C., Rijkers, R. H. B., Verbeek, J. W., and Wong, Th. E.: Subsurface structure of the Netherlands - results of recent onshore and offshore mapping, Netherlands Journal of Geosciences - Geologie en Mijnbouw, 85, 245–276, https://doi.org/10.1017/S0016774600023064, 2006.

665

Færseth, R. B.: Interaction of Permo-Triassic and Jurassic extensional fault-blocks during the development of the northern North Sea, J Geol Soc London, 153, 931–944, https://doi.org/10.1144/gsjgs.153.6.0931, 1996.

Fisher, Q. J. and Knipe, R. J.: The permeability of faults within siliciclastic petroleum reservoirs of the North Sea and
670   Norwegian Continental Shelf, Marine and Petroleum Geology, 18, 1063–1081, https://doi.org/10.1016/S0264-8172(01)00042-3, 2001.

Fossen, H., Ksienzyk, A. K., Rotevatn, A., Bauck, M. S., and Wemmer, K.: From widespread faulting to localised rifting: Evidence from K-Ar fault gouge dates from the Norwegian North Sea rift shoulder, Basin Research, 33, 1934–1953,
675   https://doi.org/10.1111/bre.12541, 2021.

Franke, D.: Rifting, lithosphere breakup and volcanism: Comparison of magma-poor and volcanic rifted margins, Mar Pet Geol, 43, 63–87, https://doi.org/10.1016/j.marpetgeo.2012.11.003, 2013.

680   Gawthorpe, R. L. and Leeder, M. R.: Tectono-sedimentary evolution of active extensional basins, Basin Research, 12, 195–218, https://doi.org/10.1111/j.1365-2117.2000.00121.x, 2000.

Geluk, M. C. and Röhling, H. G.: High-resolution sequence stratigraphy of the Lower Triassic Buntsandstein in the Netherlands and Northwestern Germany, Geologie en Mijnbouw (Geology and Mining), 76, 227–246,
685   https://doi.org/10.1023/A:1003062521373, 1997.

Geluk, M. C., Plomp, A., and van Doorn, T. H. M.: Development of the Permo-Triassic succession in the basin fringe area, southern Netherlands, in: Geology of Gas and Oil under the Netherlands, Springer Netherlands, Dordrecht, 57–78, https://doi.org/10.1007/978-94-009-0121-6_7, 1996.

690   Geothermie Nederland: Locaties op de kaart, https://geothermie.nl/geothermie/locaties-op-kaart/, last access: 25 May 2023.

Gouiza, M. and Paton, D. A.: The Role of Inherited Lithospheric Heterogeneities in Defining the Crustal Architecture of Rifted Margins and the Magmatic Budget During Continental Breakup, Geochemistry, Geophysics, Geosystems, 20, 1836–1853, 695   https://doi.org/10.1029/2018GC007808, 2019.

Harding, T. P.: Petroleum Traps Associated with Wrench Faults, Am Assoc Pet Geol Bull, 58, https://doi.org/10.1306/83D91669-16C7-11D7-8645000102C1865D, 1974.

700   den Hartog Jager, D. G.: Fluviomarine sequences in the Lower Cretaceous of the West Netherlands Basin: correlation and seismic expression, in: Geology of Gas and Oil under the Netherlands, Springer Netherlands, Dordrecht, 229–241, https://doi.org/10.1007/978-94-009-0121-6_19, 1996.

Haq, B. U., Hardenbol, J., and Vail, P. R.: Chronology of fluctuating sea levels since the Triassic, Science, 235, 1156-1167, 705   https://doi.org/10.1126/science.235.4793.1156, 1987.
Henstra, G. A., Berg Kristensen, T., Rotevatn, A., and Gawthorpe, R. L.: How do pre-existing normal faults influence rift geometry? A comparison of adjacent basins with contrasting underlying structure on the Lofoten Margin, Norway, Basin Research, 31, 1083–1097, https://doi.org/10.1111/bre.12358, 2019.

710   Henza, A. A., Withjack, M. O., and Schlische, R. W.: Normal-fault development during two phases of non-coaxial extension: An experimental study, J Struct Geol, 32, 1656–1667, https://doi.org/10.1016/j.jsg.2009.07.007, 2010.

Herngreen, G. F. W., Kouwe, W. F. P., and Wong, T. E.: The Jurassic of the Netherlands, Geological Survey of Denmark and Greenland Bulletin, 1, 217–230, https://doi.org/10.34194/geusb.v1.4652, 2003.
715

de Jager, J., Doyle, M. A., Grantham, P. J., and Mabillard, J. E.: Hydrocarbon habitat of the West Netherlands Basin, in: Geology of Gas and Oil under the Netherlands, Springer Netherlands, Dordrecht, 191–209, https://doi.org/10.1007/978-94-009-0121-6_17, 1996.

720   de Jager, J.: Inverted basins in the Netherlands, similarities and differences, Netherlands Journal of Geosciences - Geologie en Mijnbouw, 82, 339–349, https://doi.org/10.1017/S0016774600020175, 2003.

Jeremiah, J. M., Duxbury, S., and Rawson, P.: Lower Cretaceous of the southern North Sea Basins: reservoir distribution within a sequence stratigraphic framework, Netherlands Journal of Geosciences - Geologie en Mijnbouw, 89, 203–237, https://doi.org/10.1017/S0016774600000706, 2010.

Kley, J.: Timing and spatial patterns of Cretaceous and Cenozoic inversion in the Southern Permian Basin, Geological Society, London, Special Publications, 469, 19–31, https://doi.org/10.1144/SP469.12, 2018.

Kley, J. and Voigt, T.: Late Cretaceous intraplate thrusting in central Europe: Effect of Africa-Iberia-Europe convergence, not Alpine collision, Geology, 36, 839-842, https://doi.org/10.1130/G24930A.1, 2008.

Kramers, L., van Wees, J. D., Pluymaekers, M. P. D., Kronimus, A., and Boxem, T.: Direct heat resource assessment and subsurface information systems for geothermal aquifers; the Dutch perspective, Netherlands Journal of Geosciences - Geologie en Mijnbouw, 91, 637–649, https://doi.org/10.1017/S0016774600000421, 2012.

Kombrink, H., Doornenbal, J. C., Duin, E. J. T., den Dulk, M., ten Veen, J. H., and Witmans, N.: New insights into the geological structure of the Netherlands; results of a detailed mapping project, Netherlands Journal of Geosciences - Geologie en Mijnbouw, 91, 419–446, https://doi.org/10.1017/S0016774600000329, 2012.

Kortekaas, M., Böker, U., van der Kooij, C., and Jaarsma, B.: Lower Triassic reservoir development in the northern Dutch offshore, Geological Society, London, Special Publications, 469, 149-168, https://doi.org/10.1144/SP469.19, 2018.

Limberger, J., Boxem, T., Pluymaekers, M., Bruhn, D., Manzella, A., Calcagno, P., Beekman, F., Cloetingh, S., and van Wees, J. D. (2018). Geothermal energy in deep aquifers: A global assessment of the resource base for direct heat utilization, Renewable and Sustainable Energy Reviews, 82, 961-975, https://doi.org/10.1016/j.rser.2017.09.084, 2018.

Mart, Y. and Dauteuil, O.: Analogue experiments of propagation of oblique rifts, Tectonophysics, 316, 121–132, https://doi.org/10.1016/S0040-1951(99)00231-0, 2000.

McClay, K. R. and White, M. J.: Analogue modelling of orthogonal and oblique rifting, Mar Pet Geol, 12, 137–151, https://doi.org/10.1016/0264-8172(95)92835-K, 1995.

Michon, L., van Balen, R. T., Merle, O., and Pagnier, H.: The Cenozoic evolution of the Roer Valley Rift System integrated at a European scale, Tectonophysics, 367, 101–126, https://doi.org/10.1016/S0040-1951(03)00132-X, 2003.

Mijnlieff, H. F.: Introduction to the geothermal play and reservoir geology of the Netherlands, Netherlands Journal of Geosciences, 99, e2, https://doi.org/10.1017/njg.2020.2, 2020.

760   Naliboff, J. and Buiter, S. J. H.: Rift reactivation and migration during multiphase extension, Earth Planet Sci Lett, 421, 58–67, https://doi.org/10.1016/j.epsl.2015.03.050, 2015.

O'Sullivan, C. M., Childs, C. J., Saqab, M. M., Walsh, J. J., and Shannon, P. M.: Tectonostratigraphic evolution of the Slyne Basin, Solid Earth, 13, 1649–1671, https://doi.org/10.5194/se-13-1649-2022, 2022.

765

Peron-Pinvidic, G. and Manatschal, G.: Rifted Margins: State of the Art and Future Challenges, Front Earth Sci (Lausanne), 7, https://doi.org/10.3389/feart.2019.00218, 2019.

Poulsen, S. E., Balling, N., and Nielsen, S. B.: A parametric study of the thermal recharge of low enthalpy geothermal
770   reservoirs, Geothermics, 53, 464–478, https://doi.org/10.1016/j.geothermics.2014.08.003, 2015.

Racero-Baena, A. and Drake, S. J.: Structural style and reservoir development in the West Netherlands oil province, in: Geology of Gas and Oil under the Netherlands, Springer Netherlands, Dordrecht, 211–227, https://doi.org/10.1007/978-94-009-0121-6_18, 1996.

775

Riedel, W.: Zur Mechanik geologischer Brucherscheinungen ein Beitrag zum Problem der Fiederspatten, Centralblatt für Mineralogie, Geologie und Paläontologie, 354-368,1929.

Rosenbaum, G., Lister, G. S., and Duboz, C.: Relative motions of Africa, Iberia and Europe during Alpine orogeny,
780   Tectonophysics, 359, 117-129, https://doi.org/10.1016/S0040-1951(02)00442-0, 2002.
Sanderson, D. J. and Marchini, W. R. D.: Transpression, J Struct Geol, 6, 449–458, https://doi.org/10.1016/0191-8141(84)90058-0, 1984.

Sissingh, W.: Palaeozoic and Mesozoic igneous activity in the Netherlands: a tectonomagmatic review, Netherlands Journal
785   of Geosciences - Geologie en Mijnbouw, 83, 113–134, https://doi.org/10.1017/S0016774600020084, 2004.

Sylvester, A. G.: Strike-slip faults, Geol Soc Am Bull, 100, 1666–1703, https://doi.org/10.1130/0016-7606(1988)100%3C1666:SSF%3E2.3.CO;2, 1988.

790 Tari, G., Arbouille, D., Schléder, Z., and Tóth, T.: Inversion tectonics: a brief petroleum industry perspective, Solid Earth, 11, 1865-1889, https://doi.org/10.5194/se-11-1865-2020, 2020.

TNO-GDN: Stratigraphic Nomenclature of the Netherlands, https://www.dinoloket.nl/en/stratigraphic-nomenclature, last access: 10 May 2023.

795

van der Voet, E., Heijnen, L., and Reijmer, J. J. G.: Geological evolution of the Chalk Group in the northern Dutch North Sea: inversion, sedimentation and redeposition, Geol Mag, 156, 1265–1284, https://doi.org/10.1017/S0016756818000572, 2019.

Voigt, T., Kley, J., and Voigt, S.: Dawn and dusk of Late Cretaceous basin inversion in central Europe, Solid Earth, 12, 1443-
800 1471, https://doi.org/10.5194/se-12-1443-2021, 2021.

Vondrak, A. G., Donselaar, M. E., and Munsterman, D. K.: Reservoir architecture model of the Nieuwerkerk Formation (Early Cretaceous, West Netherlands Basin): diachronous development of sand-prone fluvial deposits, Geological Society, London, Special Publications, 469, 423–434, https://doi.org/10.1144/SP469.18, 2018.

805

van Wijhe, D. H.: Structural evolution of inverted basins in the Dutch offshore, Tectonophysics, 137, 171–219, https://doi.org/10.1016/0040-1951(87)90320-9, 1987.

Wilcox, R. E., Harding, T. P., and Seely D. R.: Basic Wrench Tectonics, AAPG Bulletin, 57, 74-96, 1973.
810

Willems, C. J. L.: Doublet deployment strategies for geothermal Hot Sedimentary Aquifer exploitation: Application to the Lower Cretaceous Nieuwerkerk Formation in the West Netherlands Basin, Delft University of Technology, The Netherlands, 147 pp., 2017.

815 Willems, C. J. L. and M. Nick, H.: Towards optimisation of geothermal heat recovery: An example from the West Netherlands Basin, Appl Energy, 247, 582–593, https://doi.org/10.1016/j.apenergy.2019.04.083, 2019.

Willems, C. J. L., Nick, H. M., Donselaar, M. E., Weltje, G. J., and Bruhn, D. F.: On the connectivity anisotropy in fluvial Hot Sedimentary Aquifers and its influence on geothermal doublet performance, Geothermics, 65, 222–233,
820 https://doi.org/10.1016/j.geothermics.2016.10.002, 2017a.

Willems, C. J. L., Nick, H. M., Weltje, G. J., and Bruhn, D. F.: An evaluation of interferences in heat production from low enthalpy geothermal doublets systems, Energy, 135, 500-512, https://doi.org/10.1016/j.energy.2017.06.129, 2017b.

825 Willems, C. J. L., Vondrak, A., Munsterman, D. K., Donselaar, M. E., and Mijnlieff, H. F.: Regional geothermal aquifer architecture of the fluvial Lower Cretaceous Nieuwerkerk Formation – a palynological analysis, Netherlands Journal of Geosciences, 96, 319–330, https://doi.org/10.1017/njg.2017.23, 2017c.

Willems, C. J. L., Vondrak, A., Mijnlieff, H. F., Donselaar, M. E., and van Kempen, B. M. M.: Geology of the Upper Jurassic 830 to Lower Cretaceous geothermal aquifers in the West Netherlands Basin – an overview, Netherlands Journal of Geosciences, 99, e1, https://doi.org/10.1017/njg.2020.1, 2020.

Williams, G. D., Powell, C. M., and Cooper, M. A.: Geometry and kinematics of inversion tectonics, Geological Society, London, Special Publications, 44, 3–15, https://doi.org/10.1144/GSL.SP.1989.044.01.02, 1989.
835

Wong, T. E, Batjes, D. A. J., and de Jager, J. (Eds.): Geology of the Netherlands, Royal Netherlands Academy of Arts and Sciences, Amsterdam, The Netherlands, 362 pp., ISBN 978-9069844817, 2007.

Woodcock, N. H. and Fischer, M.: Strike-slip duplexes, J Struct Geol, 8, 725–735, https://doi.org/10.1016/0191-840 8141(86)90021-0, 1986.

Worum, G. and Michon, L.: Implications of continuous structural inversion in the West Netherlands Basin for understanding controls on Palaeogene deformation in NW Europe, J Geol Soc London, 162, 73–85, https://doi.org/10.1144/0016-764904-011, 2005.
845

Worum, G., Michon, L., van Balen, R., van Wees, J., Cloetingh, S., and Pagnier, H.: Pre-Neogene controls on present-day fault activity in the West Netherlands Basin and Roer Valley Rift System (southern Netherlands): role of variations in fault orientation in a uniform low-stress regime, Quat Sci Rev, 24, 473–488, https://doi.org/10.1016/j.quascirev.2004.02.020, 2005.

850 Ziegler, P. A.: North Sea rift system, Tectonophysics, 208, 55–75, https://doi.org/10.1016/0040-1951(92)90336-5, 1992.

Zwaan, F. and Schreurs, G.: How oblique extension and structural inheritance influence rift segment interaction: Insights from 4D analog models, Interpretation, 5, SD119–SD138, https://doi.org/10.1190/INT-2016-0063.1, 2017.

855 Zwaan, F., Schreurs, G., Naliboff, J., and Buiter, S. J. H.: Insights into the effects of oblique extension on continental rift interaction from 3D analogue and numerical models, Tectonophysics, 693, 239–260, https://doi.org/10.1016/j.tecto.2016.02.036, 2016.